Measurement of the Relationship Between Oil Circulation and Compressor Lubrication in a Mobile A/C System: Part One

J. C. Drozdek, J. D. Chappell, C. Cusano, P. S. Hrnjak,
N. R. Miller, and T. A. Newell

ACRC TR-169 July 2000

For additional information:

Air Conditioning and Refrigeration Center
University of Illinois
Mechanical & Industrial Engineering Dept.
1206 West Green Street
Urbana, IL 61801

(217) 333-3115

Prepared as part of ACRC Project 92
Measurement of Oil Circulation and Compressor Lubrication in a Mobile Air Conditioning System
C. Cusano, N. R. Miller, T. A. Newell, and P. S. Hrnjak, Principal Investigators

The Air Conditioning and Refrigeration Center was founded in 1988 with a grant from the estate of Richard W. Kritzer, the founder of Peerless of America Inc. A State of Illinois Technology Challenge Grant helped build the laboratory facilities. The ACRC receives continuing support from the Richard W. Kritzer Endowment and the National Science Foundation. The following organizations have also become sponsors of the Center.

Amana Refrigeration, Inc.
Arçelik A. S.
Brazeway, Inc.
Carrier Corporation
Copeland Corporation
DaimlerChrysler Corporation
Delphi Harrison Thermal Systems
Frigidaire Company
General Electric Company
General Motors Corporation
Hill PHOENIX
Honeywell, Inc.
Hussmann Corporation
Hydro Aluminum Adrian, Inc.
Indiana Tube Corporation
Invensys Climate Controls
Lennox International, Inc.
Modine Manufacturing Co.
Parker Hannifin Corporation
Peerless of America, Inc.
The Trane Company
Thermo King Corporation
Valeo, Inc.
Visteon Automotive Systems
Whirlpool Corporation
Wolverine Tube, Inc.
York International, Inc.

For additional information:

Air Conditioning & Refrigeration Center
Mechanical & Industrial Engineering Dept.
University of Illinois
1206 West Green Street
Urbana, IL 61801

217 333 3115

Table of Contents

Chapter Page

1. Introduction 1

2. Experimental Background 2
   2.1. Using Contact Resistance as a Method to Measure Film Lubrication 2
   2.2. Swashplate Compressor Geometry and Shoe Loading Model 4
   2.3. Surface Profilometer Measurement Background 7
   2.4. Dynamic Pressure Transducer 7
   2.5. Acoustic Emission Sensor 8
   2.6. Mobile A/C Test Loop 9

3. Compressor Instrumentation 12
   3.1. Swashplate Position Sensor 12
   3.2. Measuring Contact Resistance 12
      3.2.1. Electrical contact to the piston 14
      3.2.2. Electrical contact to the shaft 15
      3.2.3. Piston isolation 15
      3.2.4. Balanced voltage divider circuit 16
      3.2.5. Data acquisition of the contact resistance signal 17
   3.3. Dynamic Pressure Transducer 18
   3.4. Acoustic Emission Sensor 19
   3.5. Data Acquisition 19
      3.5.1. HP-VEE for system operating conditions 19
      3.5.2. SoMat™ for compressor instrumentation 20

4. Data Analysis 22
   4.1. Contact Resistance Data Reduction 22
      4.1.1. Point by point averaging 22
      4.1.2. Neighbor averaging 24
      4.1.3. Threshold resistance level technique 25
   4.2. Dynamic Pressure Data Reduction 26
   4.3. Acoustic Emission Data Reduction 27

5. Experimental Test Procedures 28
5.1. Compressor Instrumentation 28
5.2. Loop Operation – Start Up Procedures 29
5.2.1. Charging the loop 30
5.2.2. Pre-heating the evaporator air loop 31
5.2.3. Separator operation 32
5.3. Varying Steady Oil Return Tests 32
5.4. Varying Compressor Speed During Steady Oil Return 33
5.5. Varying Condenser Pressure During Steady Oil Return 33

6. Instrumentation Verification Tests 35
6.1. Compressor Run-In Tests 35
6.2. Steady State Testing 38
6.3. Compressor Speed Effects On Contact Resistance 40
6.4. Condensor Air Inlet Effects On Contact Resistance 42

7. Conclusion and Additional Work 44

Bibliography 45

Appendix A: Dynamic Pressure Transducer Mounting Instructions and Mounting Block Drawing 46

Appendix B: Acoustic Emission Mounting Instructions 48

Appendix C: Michigan Scientific Drawings for Contact Resistance Instrumentation 49

Appendix D: Compressor Assembly Instructions (per Ford Motor Co.) 53

List of Figures

Page

Figure 2.1 Yoon's results of a load applied to a shoe on a spinning disk 3
Figure 2.2 (a) Calculated pressure and inertial shoe loading at idle conditions 6
Figure 2.2 (b) Calculated net shoe loading at idle conditions 6
Figure 2.3 Acoustic emission response, both raw signal and rms, on an aluminum block to an impact from a hammer 9
Figure 2.4 Loop schematic 11
Figure 3.1 Picture of instrumented compressor 13
Figure 3.2 Schematic of instrumented compressor 13
Figure 3.3 Picture of brush assembly mounted in the half opened compressor 14
Figure 3.4 Voltage divider circuit used for the contact resistance measurement 16
Figure 3.5 Measured contact resistance with and without 333 Hz filter, sampled at 5kHz 17
Figure 3.6 Measured square wave with and without 333 Hz filter, sampled at 5kHz 18
Figure 4.1 (a) Several cycles of raw contact resistance data during idling conditions, sampled at 5 kHz 23
Figure 4.1 (b) Point by point averaging results on contact resistance data shown in Figure 4.1 (a) 23
Figure 4.2 (a) Raw contact resistance data, sampled at 50 kHz 24
Figure 4.2 (b) Eleven point neighbor averaging effects on contact resistance data shown in Figure 4.2 (a) 25
Figure 4.3 Threshold resistance applied to a contact resistance signal 26
Figure 6.1 Surface profilometry results from run-in and oil shut off experiments of CR3 36
Figure 6.2 (a) Surface profilometry results of run-in experiments of CR4 37
Figure 6.2 (b) Surface profilometry results of run-in experiments of CR5 37
Figure 6.3 (a) Threshold resistance results from run-in experiments of CR4 38
Figure 6.3 (b) Threshold resistance results from run-in experiments of CR5 39
Figure 6.4 The effects of steady oil return rate on threshold resistance results 40
Figure 6.5 Compressor speed effects on threshold resistance values 41
Figure 6.6 Condensor air inlet effects on contact resistance 43
Figure A.1 Dynamic pressure transducer mounting block location on the compressor housing 47
Figure C.1 Drawing of piston grooves 49
Figure C.2 Drawing of cover for brush assembly 50

Figure C.3 Drawing of brush block 50
Figure C.4 Drawing of outer housing.....51
Figure C.5 Drawing of inner housing.....52

ABSTRACT

A study was performed on a swashplate compressor to determine the state of lubrication. Measurements of electrical resistance were taken as a primary measure of oil film lubrication at the sliding shoe/swashplate interface. Two additional sensors were used to indirectly determine the state of compressor lubrication. These included an acoustic emission sensor mounted on the outside of the compressor and a dynamic pressure transducer mounted in the swashplate cavity of the compressor.

The compressor lubrication experiments were performed on a mobile air conditioning test stand. The loop was modified to control and measure steady oil return to the compressor. Steady oil circulation conditions were controlled to determine effects of oil circulation rate, compressor speed, and condenser air inlet temperature on compressor lubrication. Furthermore, liquid refrigerant slugging and dry oil start up tests and an oil shut off test were conducted to study severe oil lubrication conditions on the compressor.

This thesis outlines the instrumentation used on the compressor to determine the state of lubrication. Also included are the steady oil circulation test results. A second thesis, written by Chappell [2000], describes the techniques used to control and measure oil circulation. In addition, the transient oil circulation test conditions are presented, including the start up conditions and the oil shut off test.

Chapter 1. Introduction

Failure of swashplate compressors in automotive air conditioning systems due to insufficient oil circulation is not well understood. The primary failure mode of swashplate compressors is scuffing at the shoe and swashplate interface.

In order to better understand the events that occur during scuffing, there is a need to study the operating conditions during failure. Several techniques were employed to determine the state of compressor lubrication during various operating conditions.

The purpose of this thesis is to describe the compressor instrumentation used to determine the state of compressor lubrication. In addition, steady state results from the contact resistance measurement technique are presented. A second thesis, written by Chappell [2000], describes how the oil circulation was monitored and presents the combined results of oil circulation and compressor lubrication during transient loop conditions.

The compressor instrumentation comprised of three independent methods to detect oil film breakdown on the swashplate surface. The measurement of contact resistance across the sliding surface interface of the shoe and swashplate was applied to the compressor. This contact resistance technique is a direct measurement of the state of lubrication at that interface. Previous work by Yoon and Cusano [1999] has shown that a substantial reduction in the resistance across this contact indicates a destruction of the protective surface layer, ultimately resulting in scuffing failure of the swashplate surface.

Acoustic emission and sound pressure data are also taken as non-intrusive methods of early failure detection. Acoustic emissions sensors have been used to detect stress waves that are generated during scuffing failure. In addition, measurement of sound pressure in the swashplate cavity may detect sliding surface interactions.

Chapter 2. Experimental Background

The primary objective of these experiments was to investigate several techniques for measuring the state of lubrication in the compressor and compare them to measured oil circulation rates. The methods described here apply to the compressor and understanding its state of lubrication. The compressor and system components this work was applied to was that of a typical mobile air conditioning system, specifically a 1994 Ford Crown Victoria, in a controlled laboratory environment. The swashplate compressor used was a current production design of the Ford model FS-10. The swashplate was made of 390 aluminum and was coated with tin. The shoes were made of 52100 steel.

Several techniques were explored to detect oil film breakdown of the swashplate compressor. The direct measurement of contact resistance to the sliding interface between the shoe and swashplate surfaces provided information that directly related to the regime of surface interactions present. Secondary techniques to determine the state of lubrication of the compressor included a dynamic pressure transducer and an acoustic emission sensor. Signals from these sensors were collected and analyzed during different lubrication conditions to determine their ability to detect oil film breakdown.

2.1. Using Contact Resistance as a Method to Measure Film Lubrication

Contact resistance as a method to measure the film between two surfaces has been used for several decades. Preliminary data from these experiments can be found in Drozdek et al. [2000]. Since the lubricant acts as an effective insulator, full hydrodynamic lubrication results in measured values of contact resistance on the order of 10^6 Ω. During boundary and mixed lubrication, when asperity interactions become significant, the measured contact resistance drops to levels that are easily measured. Mixed lubrication is achieved when most of the weight is carried by the oil film, but some asperity interactions are present. The contact resistance across the interface during this region of lubrication has been measured with the current techniques to be between 1 Ω and 100 Ω. When oil film breakdown occurs, the load becomes completely supported by the metal surface interactions. This state is known as boundary layer lubrication. During this state, the measured values of contact resistance are between 0.01 Ω and 0.1 Ω. When boundary lubrication exists at the shoe and swashplate interface, scuffing of the sliding surfaces or other compressor damage is most likely to occur. Therefore, measuring contact

resistance can determine the conditions for oil film breakdown and the conditions of scuffing failure.

Results of Yoon and Cusano [1999] agree with these data. Yoon applied the contact resistance method for measuring oil film breakdown of a sliding shoe on a rotating disk. It was shown that when oil film breakdown occurs, the contact resistance drops several orders of magnitude. These results are summarized in Figure 2.1.

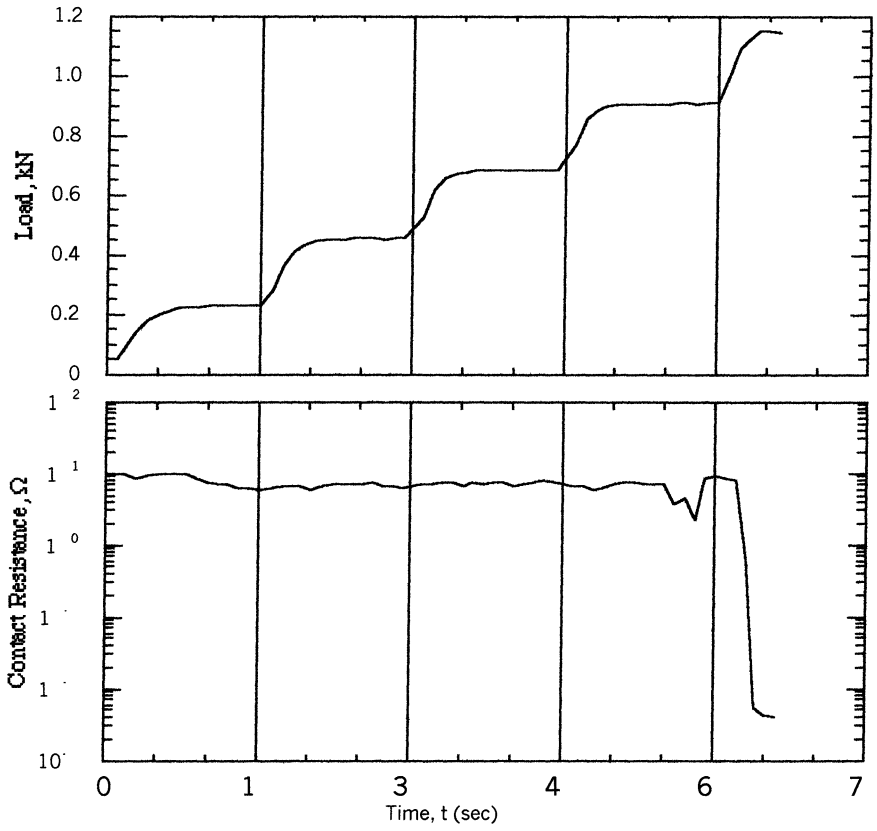

Figure 2.1 Yoon's results of a load applied to a shoe on a spinning disk

The unconditioned contact resistance signal is not smooth, instead large and abrupt changes are measured in resistance values. Furey [1961] attributed these abrupt changes in contact resistance to asperity interactions. As the two sliding surfaces begin to interact, the microscopically rough surfaces begin to interact.

For the current experiments, contact resistance was sampled at 5 and 50 kilosamples per second. Even at the highest sampling rate, large point by point variations existed due to asperity

interactions. This could indicate that the contact resistance signal was varying at a higher rate than 50 kilosamples per second.

2.2. Swashplate Compressor Geometry and Shoe Loading Model

As previously mentioned, the compressor used during these experiments was a swashplate type. The design includes five dual-sided pistons. Therefore, each rotation of the swashplate results in ten compression cycles. These compressions are a result of the shoe sliding on the rotating swashplate. The swashplate is held at a fixed angle of 21.9° to a flat disk position. The swashplate rotation causes the shoe, and therefore the piston, to travel in a sinusoidal motion governed by the swashplate motion.

Predictions of the shoe loading are necessary to distinguish signal characteristics in the contact resistance data. A simple model for the shoe loading was developed based on the predicted inertial and pressure forces applied at the shoe/swashplate interface. The inertial loading is due to the sinusoidal motion that the swashplate dictates on the mass of the piston and shoes. The pressure force on the piston is a result of the net compression of the gases in the two piston chambers.

The motion of the piston is purely sinusoidal, since the shoe travels a fixed distance from the rotating shaft and on a flat swashplate surface. From the geometry of the compressor, the position of the piston can be described with the following equation (assuming at t=0 the piston is at the top position):

$$x(t) = A\cos(\omega t)$$

Where A is half of the displacement of the piston, and ω is the speed of the compressor. The resulting acceleration of the piston and shoes can be written as:

$$a(t) = -A\omega^2 \cos(\omega t)$$

It should be noted that this acceleration is proportional to the square of the speed. Therefore, at low speeds the force contribution is small, but at higher speeds, this force becomes more significant. The inertial loading on the shoe is this acceleration multiplied by the mass of the piston and the two shoes combined (measured to be 87.9 grams). Therefore, for an idling speed of 800 rpm, the inertial shoe loading (in Newtons) becomes the following:

$$F_{inertial}(t) = -7.94\cos(8.38t)$$

The results of these inertial loads are shown in Figure 2.2 (a).

A simple model of the pressure forces has been assumed to provide insight into the loading of the shoe. This pressure force is the difference between the gases in the two

compression chambers of the piston. Beginning at the top position, the clearance volume (measured as approximately $2.0 * 10^{-7}$ m^3) in the top cylinder of the piston retains some high pressure vapor from the previous compression. As the piston moves downward, this vapor expands to the suction pressure. Once the suction pressure is achieved, it is maintained on the top cylinder of the piston until the compression cycle begins at the bottom position. The compression continues until the discharge pressure was reached, at which time the pressure on this side of the piston was maintained at the discharge pressure.

The compression of the vapor is assumed to be polytropic, such that PV^k is constant. For R-134a, a value of k=1.3 was used. Therefore, we find the following expression:

$$P_2 = P_1\left(\frac{v_1}{v_2}\right)^k$$

Two other assumptions about the reed valves were necessary to complete the model of the pressure in the cylinder. First, when refrigerant is entering the cylinder, the pressure is held constant at the suction line pressure. Second, when the pressure is compressed to the discharge pressure, the discharge valve opens and the pressure in the cylinder is held constant at the compressor discharge pressure. These assumptions disregard effects of the reed valves and compressor geometry on the pressure within the compressor.

By combining the cylinder geometry with the above pressure compression correlation, the pressure component on the shoe loading can be approximated. The result of these assumptions can be seen in Figure 2.2 (a). This figure describes the net pressure force on the piston as a result of the compression of the gas on each side of the piston. The pressure difference of 551.6 kPa (80 psi) across the compressor used in this approximation was taken from data collected during conditions where the speed of the compressor was at an idle speed of 800 rpm. The total shoe loading, the sum of the inertial and pressure forces, is described in Figure 2.2 (b).

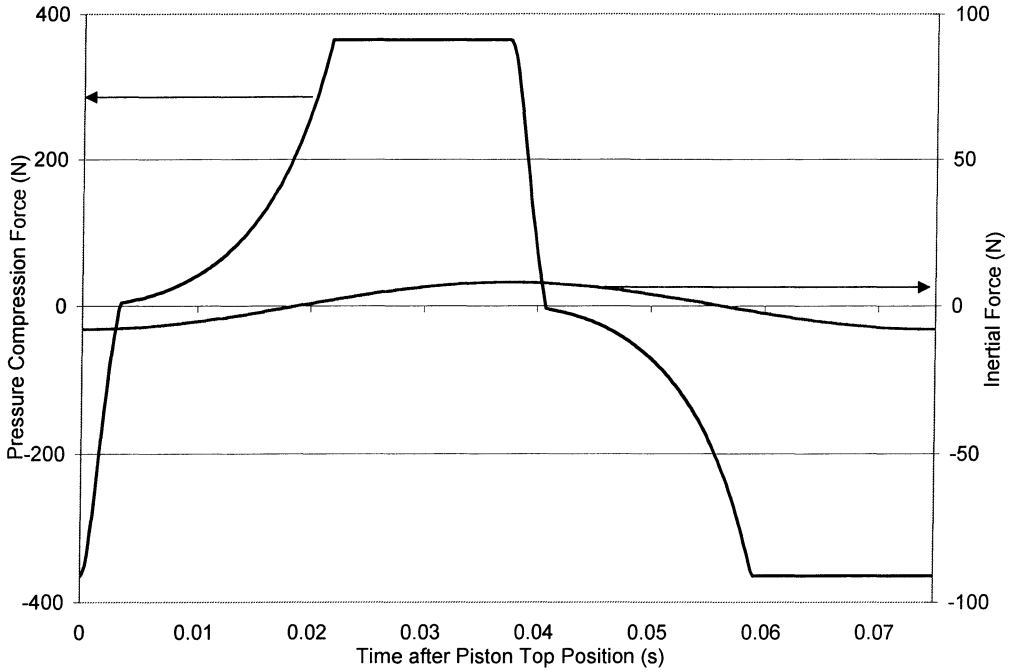

Figure 2.2 (a) Calculated pressure and inertial shoe loading at idle conditions

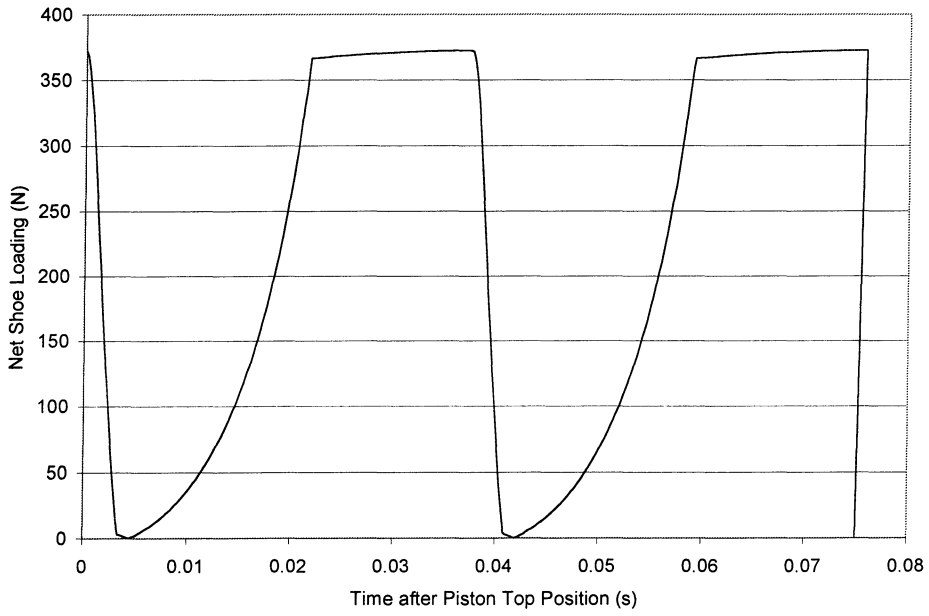

Figure 2.2 (b) Calculated net shoe loading at idle conditions

2.3. Surface Profilometer Measurement Background

Since the measured contact resistance is a measure of the interactions between two sliding surfaces, the surface roughness was measured to investigate trends as a swashplate becomes "run-in". The compressors used were purchased from the local Ford parts dealer, and therefore had seen minimal use. Initial surface profiles of the swashplate were taken as well as after several periods of operating time to investigate the run-in characteristics of the swashplate.

Surface profile measurements were made using a Sloan Dektak^3 ST stylus surface profilometer. The apparatus utilized a diamond tipped stylus to transverse the specimen and measure surface structure to within a few nanometers. The instrument was limited to profiles taken through a linear transverse. Since a continuous surface profile was unattainable, several swashplate profiles were taken in a radial direction, outward across the wear surface. The profiles were then analyzed to determine average roughness values. These average roughness values were then grouped together by location of the swashplate measurement and averaged. The groups were defined by the four following areas of the swashplate:

1) Top piston position
2) 90 degrees after top piston position
3) Bottom piston position
4) 90 degrees before top piston position

From the calculated shoe loading curves, maximum loading on the swashplate occurs in positions 4 and 1. In these locations, it is expected that the highest amount of smoothing will occur, and therefore, one could expect the lowest values of surface roughness would be found there.

2.4. Dynamic Pressure Transducer

The application of contact resistance to measure the state of compressor lubrication worked well in the laboratory. However, application of the technique as a diagnostic tool in automotive applications is less practical due to the fragility of the technique. Instead, it has been used as a fundamental technique to measure oil film thickness within the compressor. Two other more practical techniques were investigated for their potential application as a system diagnostic in automotive applications: a dynamic pressure transducer and an acoustic emission sensor. These methods are more robust than the method of contact resistance, and therefore, more readily applied to an automotive environment.

The dynamic pressure transducer is based on the idea that during scuffing failure noise will be generated. As a result, the transducer was mounted in the internal cavity of the compressor to monitor sound pressure events generated near the shoe/swashplate interface.

This method used a dynamic pressure transducer capable of withstanding the pressures present in the compressor cavity, yet maintained high sensitivity to changes in the pressure. The model of transducer used was a PCB Piezoelectronics subminiature pressure transducer, catalog number 105B02. The specifications of this sensor can be found in Appendix A. The dynamic pressure transducer data were acquired at 50 kilosamples per second with the same hardware as the contact resistance measurement.

2.5. Acoustic Emission Sensor

The other non-intrusive method for detecting oil film breakdown is the acoustic emission sensor. The method of acoustic emission has been successful in detecting oil film breakdown and scuffing in engine bearings (Kioke et al. [1998]). The acoustic emissions detected are generated from the local scuffing failures associated with oil film breakdown. The resulting stress waves travel through the material and can become surface waves when they reach the surface. These surface waves can have a frequency as high as 1 megahertz. As a result, they can be attenuated easily. However, if good acoustic coupling is achieved, an acoustic emissions sensor can easily detect this signal.

The acoustic emission sensor, the Physical Acoustics Corp. model R15, was used to detect high frequency acoustic emissions on the surface of the compressor. Specifications of this sensor can be found in Appendix B. Data for the acoustic sensor were acquired with a digitizing oscilloscope with a maximum bandwidth of 100 MHz. Unfortunately, since only once screen of data can be captured at a time, this method has a very limited sampling window size. With a screen length of 500 pixels and sampling at 1 MHz gives a sampling window of 0.0005 seconds. This was an unacceptable window length to compare events occurring through a cycle of length 0.08 seconds.

An alternative output channel of the acoustic emission signal conditioner was the root mean square (RMS) value of the acoustic emission signal. This RMS signal was sampled at 50 kHz with the same hardware as the contact resistance and pressure microphone signals.

A simple test was performed to determine the RMS signal's response to an impulse. The test was performed using an aluminum block that was impacted with a hammer on one end. On the other end the acoustic emission sensor detected the event. This test produced the impulse

response of the sensor. Both the raw signal and the RMS output were simultaneously recorded from this event. The results of this test are included in Figure 2.3. The sharp rise in the RMS signal caused by the signal indicates when the signal occurred. The slow decay of the RMS signal significantly increases the duration of the signal. Therefore, by using the RMS output of the acoustic emission sensor, impulses from the sensor can be detected using a slower sampling rate than necessary to collect the high frequency raw signal characteristics. As a result, the RMS signal was recorded at 50 kHz using the same hardware as described in the previous compressor instrumentation descriptions.

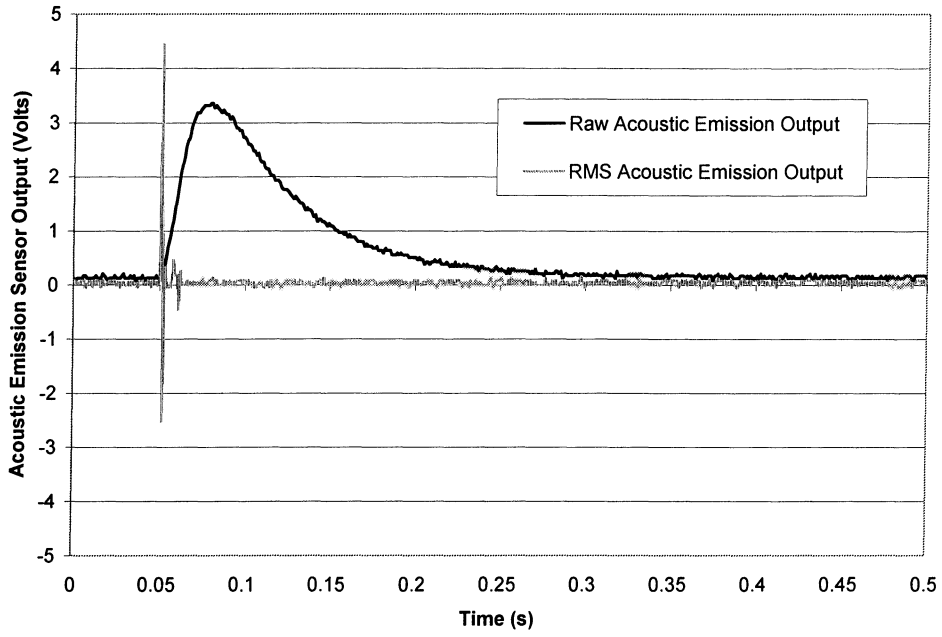

Figure 2.3 Acoustic emission response, both raw signal and rms, on an aluminum block to an impact from a hammer

2.6. Mobile A/C Test Loop

The tests were performed on the mobile air conditioning test stand at the University of Illinois Air Conditioning and Refrigeration Center. The test stand was built by Weston et al. [1996], and it was designed to simulate mobile loop conditions and measure system performance variables for different automotive components, i.e. exchanging out the compressor and measuring COP. Therefore, the loop has been fully instrumented to measure temperature and pressure throughout. Also, two wind tunnels control the condenser and evaporator air side flow rates. The blower speed of both air loops and the compressor drive motor are controlled with variable speed drives for accurate reproduction of driving conditions. The current configuration

of the loop includes system components of a 1994 Ford Crown Victoria air conditioning system. This includes a fixed orifice expansion device, a suction line accumulator, and a swashplate compressor.

Since multiphase flow exists throughout most of the air conditioning loop, current techniques to measure oil lubrication are limited to the liquid line, where only liquid refrigerant is present. Typically, oil circulation rate is measured using a mass flow meter in the liquid line in conjunction with a method to determine the concentration of oil in the refrigerant. Together these measurements allow the mass flow rate of oil to be calculated.

A common approach for measuring concentration is to have sampling sections in the liquid line available so that a sample can be pulled when a measurement is desired. Other in-line techniques have been investigated. Meyer and Jabardo [1994] investigated the use of the change in the speed of sound through the mixture of oil and refrigerant. However, this method was very sensitive to vapor bubbles entrained in the flow. Wandell et al. [1997] utilized the change in refractive index of the oil and refrigerant mixture to determine the concentration of oil in refrigerant. This work was done on the same test stand where the current tests were performed, and the liquid line concentration was known and measured during these experiments. Their experiments investigated transient oil return rates, but since they were limited to the liquid line, they could not describe what was returning to the compressor.

To investigate oil circulation at the suction to the compressor, modifications to the current loop design were necessary. To control oil mass flow in the suction line, the oil was separated from the returning vapor flow. This oil flow was then metered back into the suction line. The additional oil return line added to the loop can be seen in Figure 2.4.

The separator used was a helical type that is most commonly found in stationary air conditioning systems where the oil is separated at the compressor discharge and re-circulated back to the sump of the compressor. The helical shape in the separator causes the oil to be forced to the outside of the separator where it collects on the wall and slowly flows to the base of the separator. Meanwhile, the lightweight refrigerant vapor passes through the helical shape with little pressure drop.

The oil in the oil return line has refrigerant mixed in it due to the refrigerant rich environment. Therefore, the concentration of liquid refrigerant in oil must be measured to calculate the oil mass flow rate. The concentration sensor used was similar in design to what Wandell et al. [1997] had used. Both devices react to changes in refractive index of the mixture and then are related to the concentration of the mixture measured in situ. The previous design

used a glass window, with a refractive index of 1.58, to detect changes in refractive index. However, this material was limited to low concentrations of oil in refrigerant. The new design uses a sapphire window, with a refractive index of 1.75, as the optic media. The higher refractive index of sapphire increased the range of sensitivity so that all mixtures of refrigerant in oil could be measured.

The mass flow rate of the oil return line is determined with a mass flow meter, MicroMotion© model UMF-10. The flow is controlled with a pressure drop valve and a controlling needle valve, as seen in Figure 2.4.

After the oil has been separated, its concentration of refrigerant measured, and the mass flow rate measured, it flows through a sampling section that was used during the in situ calibration of the concentration sensor. Finally, the oil flows through a controlling needle valve, and then is re-mixed with the refrigerant vapor flow returning to the compressor.

The result of the oil return line is control of steady oil flow returning to the compressor. Therefore, by combining the compressor instrumentation and the oil return rate, the state of compressor lubrication can be correlated to levels of oil circulation during steady conditions. A more detailed description of these methods used to control and measure oil circulation can be found in Chappell [2000].

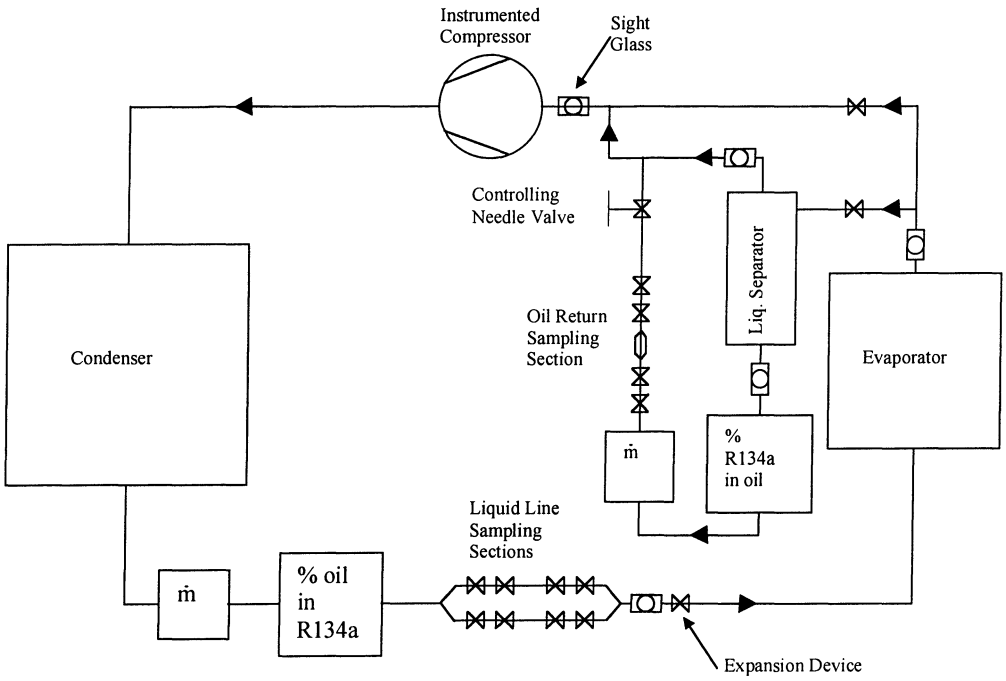

Figure 2.4 Loop schematic

Chapter 3. Compressor Instrumentation

The instrumentation of the compressor was designed such that simultaneous data could be collected to relate the output of the aforementioned sensors to the position of the pistons as well as the condition the loop was running in. The compressor instrumentation required sampling at a very high rate, which was not attainable with the existing HP-VEE based data collection system. Therefore, a data acquisition system capable of high sampling rates was necessary for the compressor instrumentation data to be collected. The data acquisition system used for the compressor instrumentation was a SoMat™ mobile data collection system.

3.1. Swashplate Position Sensor

A simultaneous input of swashplate position was necessary to apply the calculated shoe loading approximations to the measurements of contact resistance. To record swashplate position, the combination of a fiber optic sensor and a reflective flag on the clutch assembly was used. The optic sensor used was a Honeywell micro switch, model HPX-F1-H. The location of this sensor can be seen in Figure 3.1. The output was digital and was activated when the reflective flag passed in front of the sensor. Since the flag was mounted to the clutch, it could be related to the position of the swashplate. The flag was a small piece of metal covered with reflective aluminum foil tape. The flag extended past the outer diameter of the clutch so that the only surface to pass in front of the optic sensor was the reflective flag. The flag and optic sensor were positioned such that the beginning of the generated pulse corresponded to the instrumented piston at top center position.

3.2. Measuring Contact Resistance

In order to measure the electrical contact resistance across the shoe and swashplate interface, a circuit was designed through the compressor to isolate this resistance. A schematic drawing of the compressor and the instrumentation used to determine the state of compressor lubrication is shown in Figure 3.2.

The circuit used to measure contact resistance at the shoe/swashplate interface needed to connect through the compressor. It began with a brush assembly that was mounted to the outer housing of the compressor that could pass several insulated wires through the outer housing so that contact to the piston could be obtained. Since the piston was in constant motion, a sliding contact was mounted on the side of the piston. The pistons are ringed with an electrically

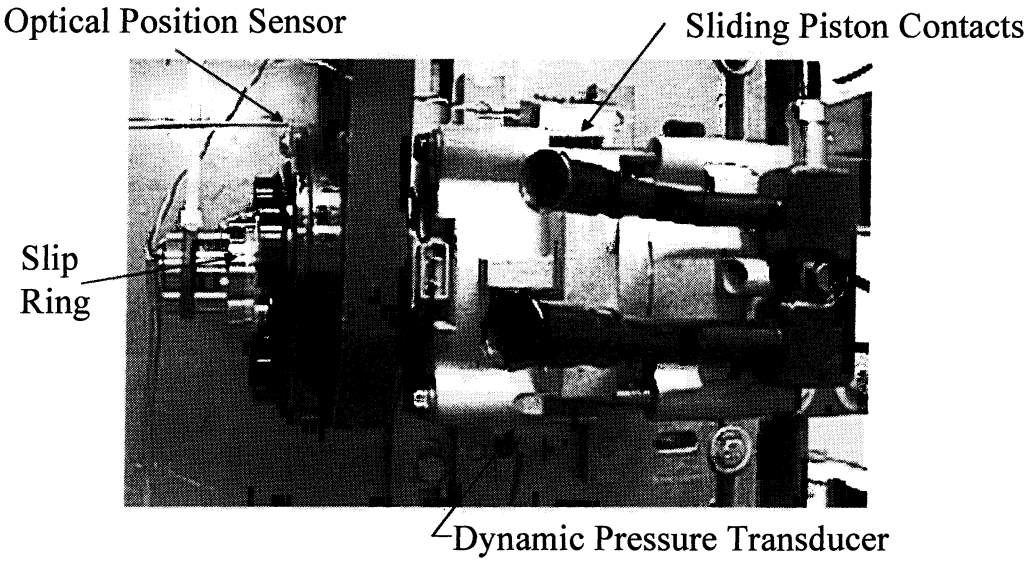

Figure 3.1 Picture of instrumented compressor

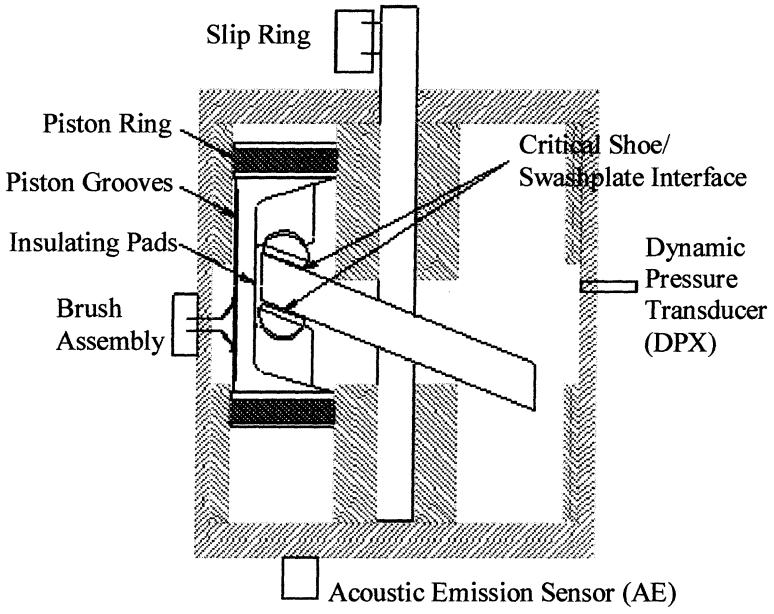

Figure 3.2 Schematic of instrumented compressor

insulating material so that a short circuit could not occur between the piston and compressor housing. Also, the region of the piston that connects the two ends, referred to as the piston bridge, can come into contact with the edge of the swashplate and short the contact resistance measurement at the shoe/swashplate interface. Therefore, care was taken to isolate the piston bridge from the edge of the swashplate by the addition of inlaid non-conducting polymer pads in the piston bridge. The area of contact from the piston to the shoe is small, and therefore the

resulting resistance from this interface is small. From the shoe, the circuit passes across the critical shoe and swashplate interface where the contact resistance will be measured. From the shoe/swashplate interface, the circuit continues to the swashplate, then to the shaft, and finally through a slip ring on the end of the shaft. This slip ring is the second contact point of the circuit outside the compressor.

3.2.1. Electrical contact to the piston

The method for maintaining a sliding contact to the piston includes a series of grooves machined in the piston, which allows metal brushes to ride in them and maintain electrical contact. It was desired to add gold plating to the surface of the piston to maintain a higher quality sliding electrical connection. However, the gold was not easily plated to the aluminum alloy, so instead an intermediate layer of nickel plating was used. The nickel was plated on the piston, and then the gold was plated on the nickel.

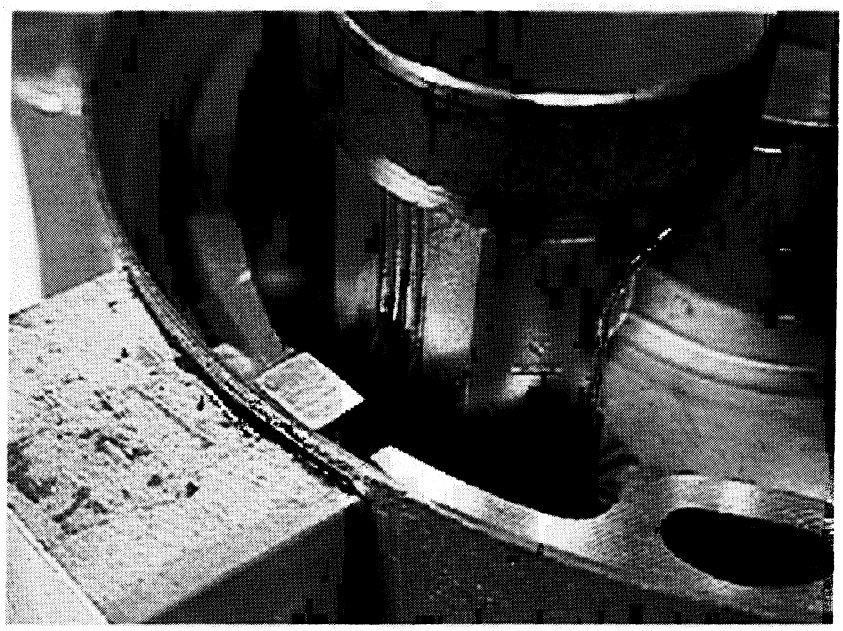

Figure 3.3 Picture of brush assembly mounted in the half opened compressor

The brush and groove assembly was designed by Michigan Scientific, a company that manufactures slip rings and whose expertise is in sliding electrical contacts. The drawings provided by Michigan Scientific for this brush mounting technique are included in Appendix C. The brush assembly contains eight pairs of metal brushes lay in the piston grooves, two pairs for each groove. Therefore, there are sixteen fingers maintaining electrical contact to the piston. Half of the brushes were used to apply the voltage in the contact resistance circuit, and the

remaining brushes were used to measure the voltage across the contact resistance of the critical sliding shoe and swashplate interface of interest. A picture of the top of the brush assembly, i.e. eight fingers, can be seen in Figure 3.3. Also visible are the grooves and plating performed on the piston.

3.2.2. Electrical contact to the shaft

To maintain electrical contact to the rotating shaft of the compressor, a four-circuit slip ring was used. Although only one contact was necessary to build the contact resistance circuit, all four contacts were used to decrease the chance of malfunction. The slip ring was manufactured by Michigan Scientific, model number S4. Similar to the electrical contact to the piston, the slip ring used four sets of brushes to establish a good electrical contact. An aluminum block was machined to mount the slip ring to the end of the shaft. The mounting block attached to the clutch and shaft, and the slip ring was attached to the mounting block. Wires from the slip ring were soldering together into a single node on the mounting block. Therefore, electrical contact was maintained through the slip ring, mounting block, shaft, and finally to the swashplate.

3.2.3. Piston isolation

The electrical circuit coming through the piston could short circuit to the shaft through two paths. The first was across the piston rings, that is, through the piston head and to the cylinder walls. The existing pistons were ringed with an electrically insulating material and the resistance from the piston to the bore was measured greater than 3 MΩ.

The second path to short circuit the shoe/swashplate contact resistance was from the piston bridge to the swashplate. The piston bridge is the length of the piston that connects the two ends together. In the piston bridge area, the piston can touch the swashplate and short circuit the measurement of contact resistance at the sliding shoe/swashplate interface. The force that causes the piston rotation is a result of a differential in sliding velocity between the shoe and swashplate at different locations on the swashplate. At the outermost area on the swashplate, the sliding velocity between the shoe and the swashplate is a maximum, and decreases closer to the shaft. Since this twisting force applied to the piston could not be eliminated, the short circuit between the piston bridge and the swashplate must be eliminated.

A method for electrically insulating the piston bridge contact area was developed. To maintain sufficient strength in the piston bridge, 0.5 mm of the piston bridge material was

removed from each side of the piston bridge to adhere insulating material to the piston bridge. This insulating material prevented the contact resistance circuit from short circuiting to the swashplate. Within the recessed area of the piston bridge, several materials were tested. The epoxies that were tested all failed. The surface of the epoxy could not match the smoothness of the original piston bridge, making the surface interactions between the bridge and swashplate edge more severe. The most effective method found was to epoxy a 0.5 mm thick piece of Teflon™ in the machined recess on the piston bridge. Despite the low wear resistance of this material, its low coefficient of friction kept the load on the wearing surfaces low and successfully protected both. These insulated pads proved effective during the severe tests performed on the compressors where failure due to loss of lubricant was forced. The epoxy used for these pads was a commercial 2 hour quick setting epoxy.

Observations of two failed swashplates without the Teflon™ pads in the piston bridges indicated significant interaction between the swashplate and piston bridge. Since the increase in surface roughness on the swashplate from these non-instrumented pistons would cause the Teflon™ pad on the instrumented piston to wear out more quickly. Therefore, Teflon™ pads were inlaid in all of the piston bridges in the compressor to avoid this problem.

3.2.4. Balanced voltage divider circuit

The circuit used to measure contact resistance is shown in Figure 3.4. The voltage applied to the contact resistance circuit was 1 volt. The applied voltage was balanced, that is, the voltage was applied as + 0.5 V and - 0.5 V to reduce noise generation. The maximum current the SoMat™ could provide is 28 mA. Two 25 Ω resisters were placed in series with the contact resistance to ensure the current draw did not exceed 20 mA. This also gave good data resolution for the contact resistance values of interest below 100 Ω to levels near 1 Ω.

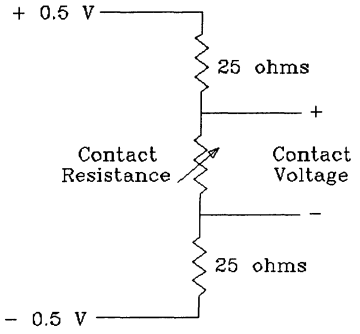

Figure 3.4 Voltage divider circuit used for the contact resistance measurement

3.2.5. Data acquisition of the contact resistance signal

The data collection equipment contained signal filters to reduce the effects of noise. However, the characteristics of the measured contact voltage can change rapidly due to asperity interactions. Several initial tests indicated the use of filters on the contact voltage data to have negative effects. This problem occurs due to the ringing response a filter has to a step change in the voltage signal. A comparison of two simultaneous voltage signals captured with and without the filter can be seen in Figure 3.5. The effects of the filter ringing are most evident when the values change quickly near 1 volt, since the effect of the ringing filter will result in voltages higher than 1 volt. Also, where the resistance is varying, the filtered signal appears smoothed out.

To provide additional information about the ringing of the filter, a square wave generator was used to provide a square wave input to the data collection hardware. The results of this test can be seen in Figure 3.6. The result of the step change present during a square wave was the "ringing" of the filtered both before and after the step change. It was determined the effects of using a filter while collecting the contact resistance data significantly altered the data in an undesirable way. As a result, all contact voltage measurements were collected without a filter.

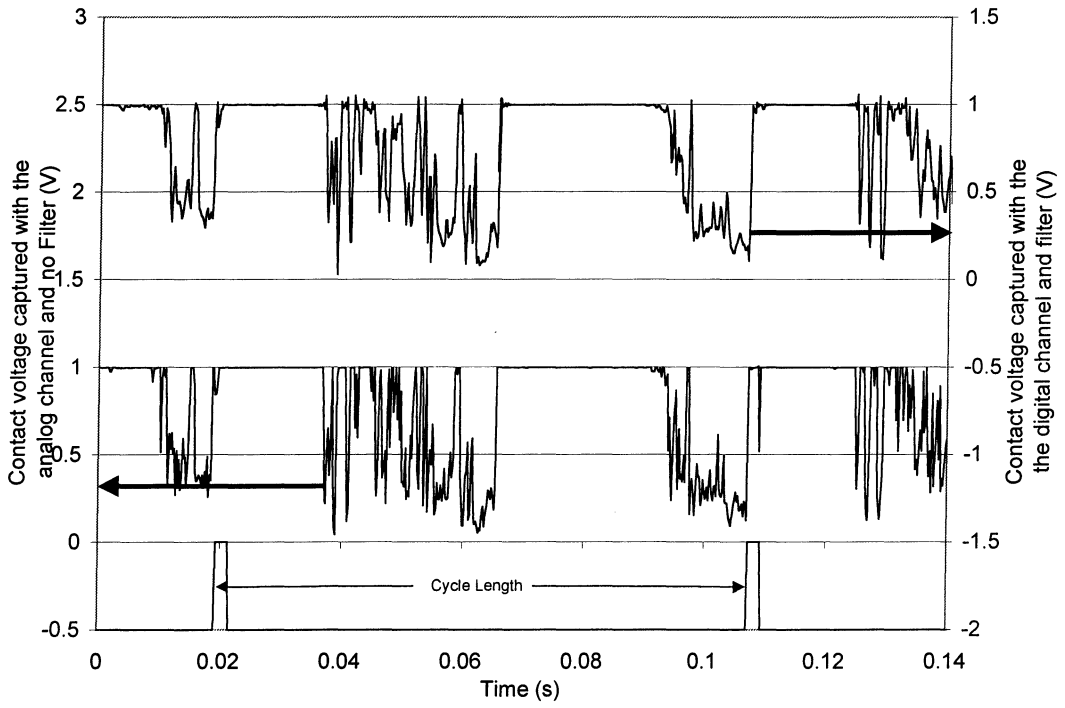

Figure 3.5 Measured contact resistance with and without 333 Hz filter, sampled at 5kHz

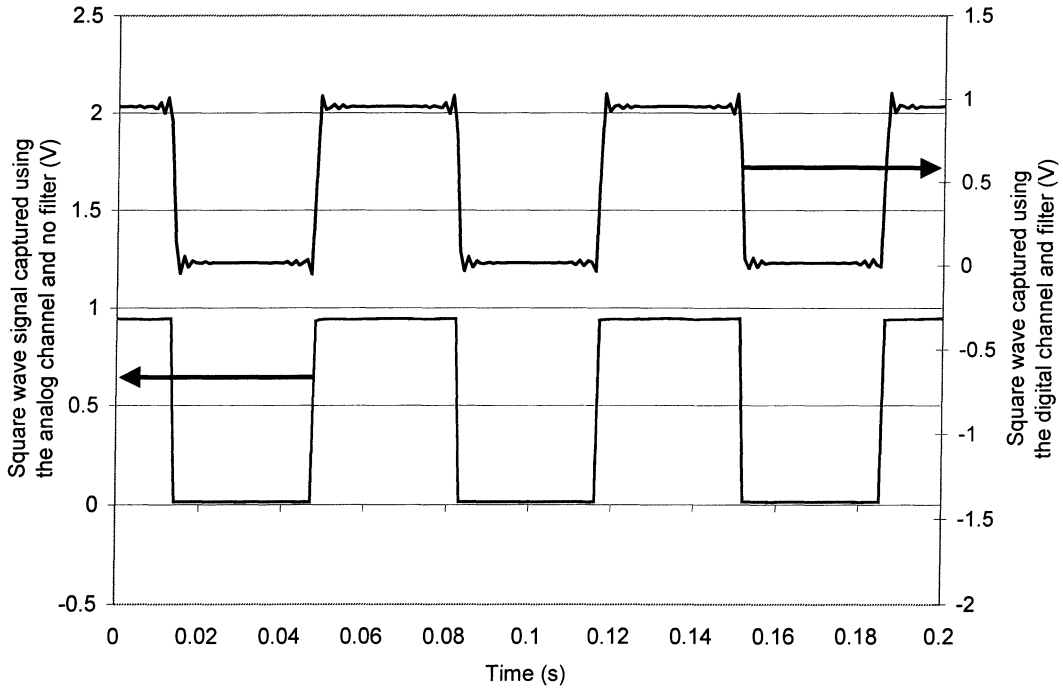

Figure 3.6 Measured square wave with and without 333 Hz filter, sampled at 5kHz

3.3. Dynamic Pressure Transducer

The strategic mounting of the dynamic pressure transducer involved mostly location constraints. The size of the microphone and microphone block are small, as described in Appendix A. However, the transducer must be mounted near the source of the signal for the greatest sensitivity. The sensor could easily be mounted flush with the outer housing, but the inner housing would continue to block good signal sensitivity. Fortunately, there are several openings in the inner housing where the sensor could be placed and have good exposure to the signal source. This opening in the inner housing corresponded to a position on the compressor in between two pistons, so there was a direct exposure of the sensor to the swashplate. It was located on the opposite side of the compressor to the contact resistance block. The approximate location of the sensor on the compressor housing is described in Figures 3.1 and A.1.

An aluminum block was machined to mount the dynamic pressure transducer in the desired location on the outer housing. Before mounting the block, a small patch on the outer housing was machined flat for good o-ring sealing. The o-rings used were made of Neoprene© so that no corrosion would take place in the R-134a environment. The block was fastened with

two bolts from the inside of the compressor into machined threads in the block. The bolt heads were recessed in the outer housing to avoid interference with the inner housing during assembly.

3.4. Acoustic Emission Sensor

The mounting of the acoustic emission sensor was quite simple. The sensor detects surface stress waves that result from surface interactions. The source of these interactions is the swashplate, and therefore, the swashplate is an ideal location to mount the sensor. However, space constraints on the swashplate did not permit this. Also, the characteristic high frequency signal could not be passed out of the compressor on a slip ring connection. The nearest feasible location for the sensor was on the outside of the compressor, mounted on the bottom. The signal would have to pass from the swashplate, through a set of bearings, through the inner housing, and finally to the outer housing. Since the signal had to pass through so many interfaces to be detected, it was likely that any signal detected would have been greatly reduced. The sensor was mounted in a small area machined flat on the bottom of the compressor. A block of wood was used to hold the sensor lightly in place. Another potential problem exists for this sensor. The housing was mounted to the same structure as the drive motor for the compressor. Therefore, events emitted from the drive motor may also be detected with this sensor. The approximate location of the sensor is shown in Figure 3.2. Mounting instructions for the sensor can be found in Appendix B.

3.5. Data Acquisition

3.5.1. HP-VEE for system operating conditions

A Hewlett-Packard data acquisition system 1300A VXI mainframe was used to collect system operating conditions. A PC used HP-VEE software to collect and view system operating conditions. For example, refrigerant and air temperatures are taken at the inlet and outlet of all major system components. The existing system has been described in more detail in Weston et al. [1994]. Three new parameters were added to the existing data acquisition system: oil return mass flow rate, oil return density, and oil return concentration sensor. In addition, the output from the program file was modified to include a description of the file names. For the high frequency acoustic emission sensor data, the digitizing scope was interfaced with HP-VEE so that captured screens would be stored with the HP-VEE clock time. This allowed the system operating conditions to be associated with compressor signals.

A digitizing oscilloscope was used to record the high frequency data of the acoustic emission sensor. The oscilloscope was a Tektronix TDS 410A and was capable of digitizing what was viewed on its 500 pixel wide screen. The maximum sampling rate of the scope was 1 GHz, which provided sufficient sampling of all acoustic emission frequencies. Unfortunately, the limitation that only one screen length could be digitized became problematic. The acoustic signal captured appeared to be time varying. Therefore, it was necessary to sample a significant portion of the cycle length to capture signal dynamics. To capture one cycle at a compressor speed of 800 rpm, the 500 data points captured are sampled at approximately 6700 samples per second. Therefore, any signal that was recorded could not be analyzed for frequency content. This technique was still used to investigate the characteristics of one acoustic event, but was not used to detect changes in the acoustic emission signal due to its sampling rate limitations.

The Tektronix signal was linked to the HP-VEE data acquisition system using the HP-IB interface card in the PC that is shared with the HP data acquisition hardware. This allowed the HP-VEE software to sample both systems and to correlate the time samples from both systems were taken to each other. Therefore, system operation could be linked to changes in the acoustic emission sensor.

3.5.2. SoMat™ for compressor instrumentation

The SoMat™ 2500 data collection system was used to capture short windows of high frequency data sets of the compressor instrumentation devices. These devices included the contact voltage measurement, the dynamic pressure transducer, the swashplate position sensor, and the RMS of the acoustic emission sensor. As previously discussed, the acoustic emission sensor was a high frequency signal and was captured using the above technique. However, the use of the RMS signal could allow simultaneous measurements of all compressor instrumentation to link events together and observe trends in the data more easily.

The final choice for sampling rate for the SoMat™ was 50 kHz. This was chosen to sample at a high enough rate to prevent aliasing of the dynamic pressure transducer data. The highest frequency apparent in this data is approximately 10 kHz. The length of the data set was limited to memory capabilities of the SoMat™, which could hold a maximum of 8 MB. While collecting all four channels of data, these "windows" of data could be collected for approximately 13 seconds. Therefore, to observe trends in the data, these windows were taken at appropriate time intervals. For example, steady state conditions were analyzed by collecting a

window of data every fifteen minutes. In between windows, the data was uploaded from the SoMat™ data acquisition hardware to a PC.

The software used to convert the SoMat™ information files (.SIF) into text files (.TXT) was SoMat™ EASE Version 3.0. This software was also capable of viewing and manipulating the data. The data could then be exported as a text file. Finally, the text file could be imported into a spreadsheet (Microsoft Excel was used) and the data could be further analyzed.

For most channels of the SoMat™ data acquisition system, digital filters were used to produce good quality signals. As previously describe, the filter must be completely removed to capture the contact resistance measurement. The only channel with this capability was the analog channel, and so it was used for the contact resistance measurements. The dynamic pressure transducer and the RMS of the acoustic emission sensor were collected at a sampling rate of 50 kHz, using digital filters with a cut off frequency of 14.5 kHz.

Chapter 4. Data Analysis

Several methods were used to manipulate the compressor data to a form that demonstrated trends within the data. The contact resistance data was reduced using two averaging schemes and a threshold level analysis. The pressure microphone and acoustic emission data were reduced using Fast Fourier Transform, FFT. However, due to the time varying characteristics of these data, these techniques were not effective at distinguishing differences among the signals. Lastly, preliminary wavelet analysis was applied to the pressure microphone data to detect specific signal characteristics and how they changed during various tests.

4.1. Contact Resistance Data Reduction

The data collected was in the form of contact voltage, and must be converted into contact resistance. Using the principles of a voltage divider circuit, the following expression was developed to calculate the contact resistance, CR, from the measured contact voltage, CV:

$$CR = 50\left(\frac{CV}{1-CV}\right)$$

Contact resistance measurements taken during various conditions are difficult to compare. Although the basic structure of the cyclic signal was repeated, the sharp changes due to surface interactions vary as the two surfaces interact and change. Therefore, additional reduction techniques were necessary to distinguish trends in the data. Several techniques were applied to the data, and are described here.

4.1.1. Point by point averaging

The overall structure of the contact resistance signal was important to observe changes in the signal. Due to the rapid fluctuations of the raw data, it was difficult to detect visual changes in the signal. Therefore, an average of many cycles was produced to observe trends in the data. Since the position sensor on the clutch distinguished each cycle, the cycles were separated. By averaging each point of one cycle with the same point from other cycles, an average cycle was obtained. The average obtained was compared to averages obtained during other operating conditions to compare the trends in the data. This method was applied to data sampled at 5 kHz and was used to average over approximately 100 cycles of data.

Several cycles of contact resistance data that have not been modified can be seen in Figure 4.1 (a). The overall structure does not change from cycle to cycle. A point by point average of the same data is shown in Figure 4.1 (b). The averaging produced a curve with much less variation and could be more easily compared to signals at other operating conditions.

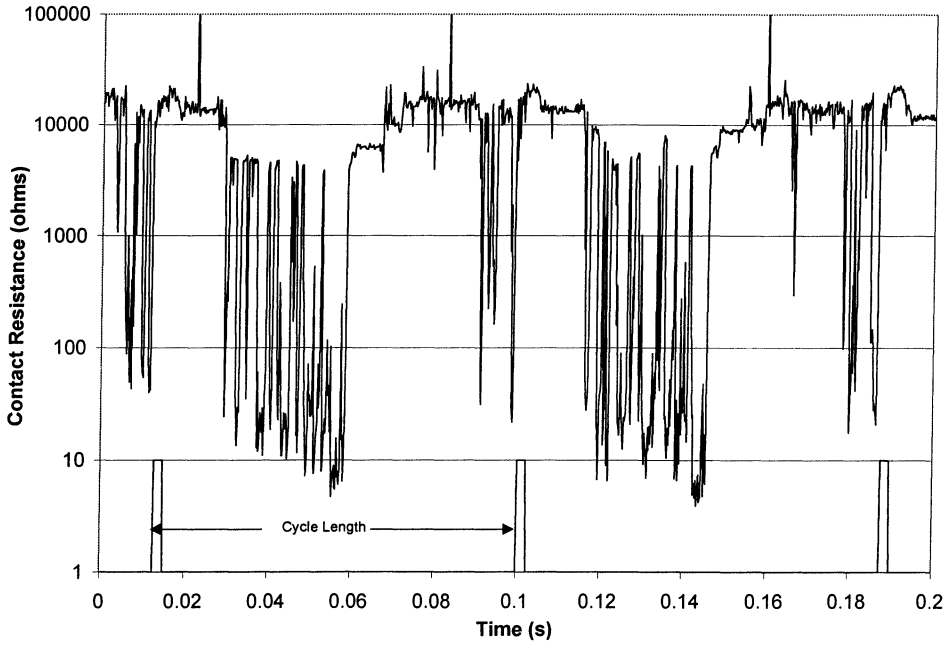

Figure 4.1 (a) Several cycles of raw contact resistance data during idling conditions, sampled at 5 kHz

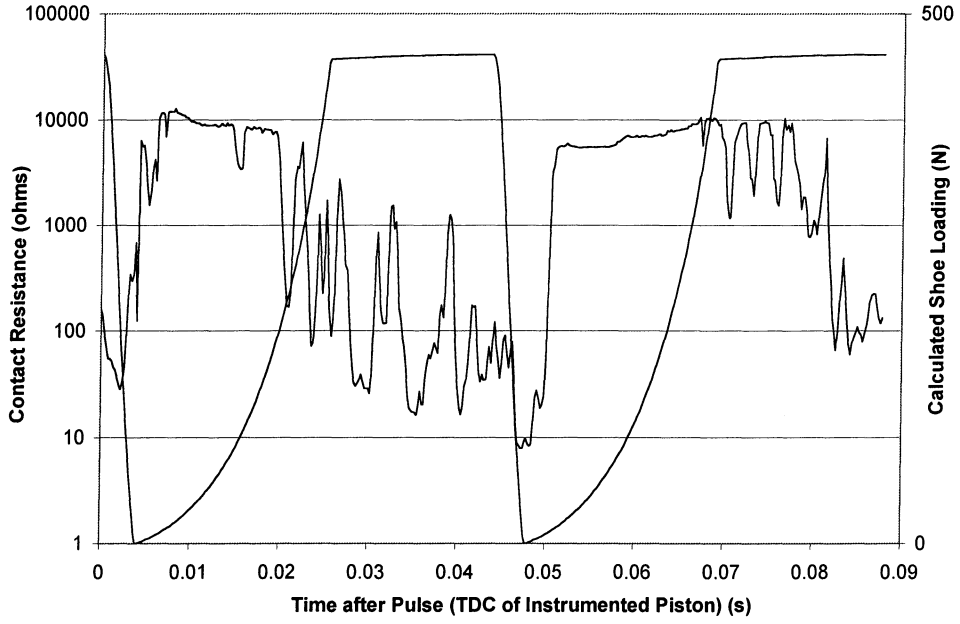

Figure 4.1 (b) Point by point averaging results on contact resistance data shown in Figure 4.1 (a)

4.1.2. Neighbor averaging

The results of point by point averaging were effective for data sampled at 5 kHz, however it was desired to sample contact resistance simultaneously with dynamic pressure, which required a sampling rate of 50 kHz. Unfortunately, limitations of the spreadsheet software could not effectively manipulate this quantity of data. Therefore other techniques were necessary. The first chosen was to average the ten neighboring data points for each point. Therefore, eleven points were averaged: the five prior to the point, the five after, and the original data point. The result was that sharp changes in resistance were less significant.

The results of neighbor averaging on contact resistance data sampled at 50 kHz have been provided in Figure 4.2 (a-b). The raw data showed large fluctuations in contact resistance, where the neighbor average describes the overall trend in the signal. This technique described the characteristics of only one cycle, instead of an average of many cycles. Therefore, cyclic variations could not be averaged out of the representation, like the point-by-point average could.

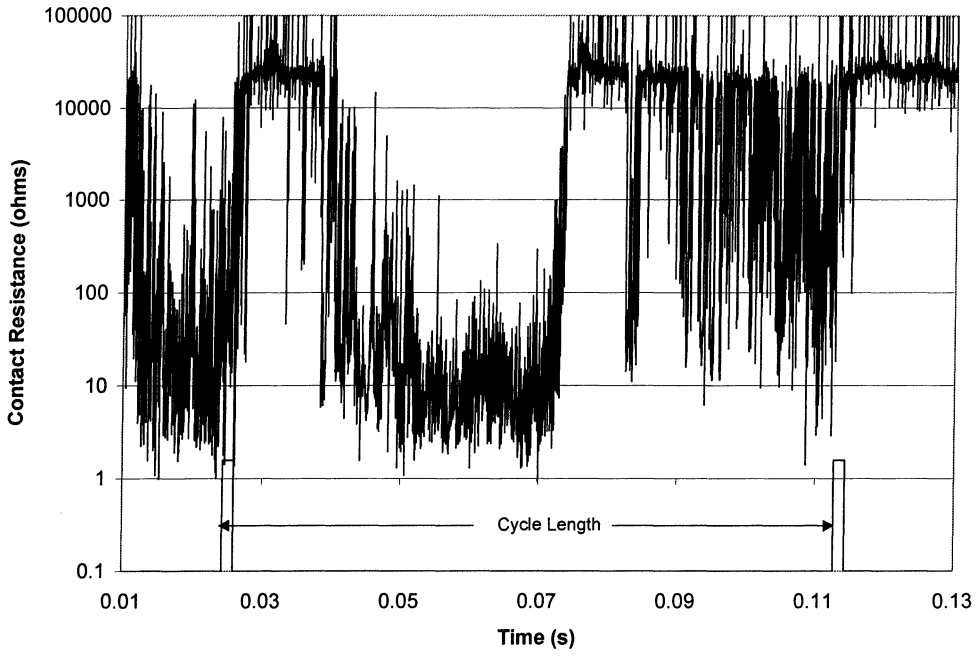

Figure 4.2 (a) Raw contact resistance data, sampled at 50 kHz

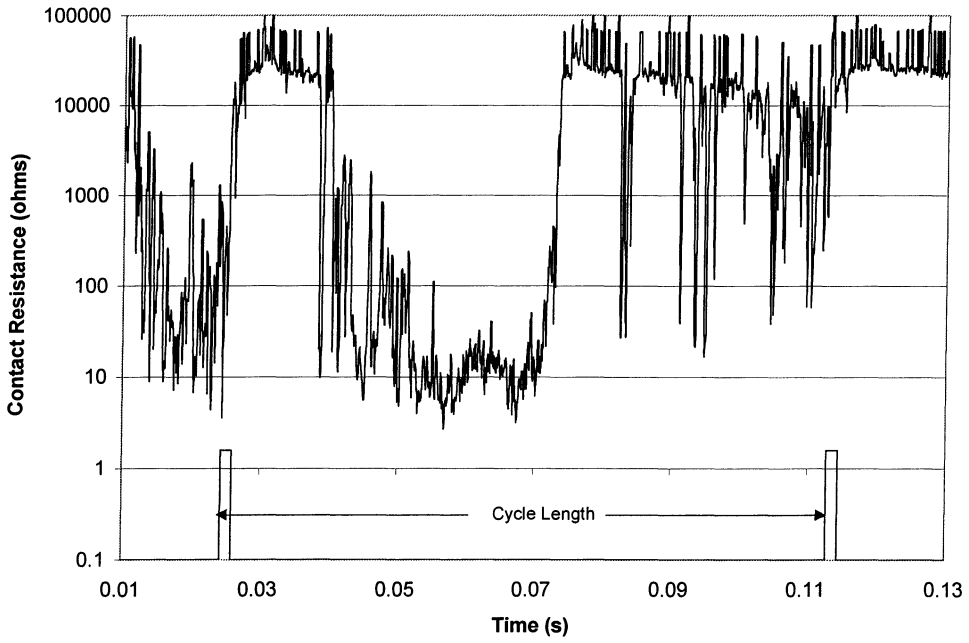

Figure 4.2 (b) Eleven point neighbor averaging effects on contact resistance data shown in Figure 4.2 (a)

4.1.3. Threshold resistance level technique

Due to the abrupt changes in measuring contact resistance, it is good to analyze the signal using other methods besides averaging. For example, Furey [1961] used a percent time technique to illustrate changes in the levels of contact resistance. There, the percent time referred to the time the signal was at low values of resistance, instead of the high values obtained during good hydrodynamic lubrication.

The current experiments compare different operating conditions, so that the lower values of resistance are compared to describe the amount of surface interaction that exist. The lower contact resistance correlated with more surface interactions, and the more time spent at these low values of resistance correlates with how much of the swashplate is experiencing high amounts of surface interaction. For example, it is known that at high levels of surface interactions take place when the contact resistance is below 1 Ω. As a result, the amount of time the signal is below 1 Ω describes how much of this severe surface interaction is occurring. The percent time the resistance was below certain threshold levels was calculated for approximately one second of data. This correlates to approximately 13 revolutions of the swashplate. The resulting percent time values for each threshold resistance were then compared to other operating conditions.

Therefore, changes in the amount of surface interaction could be attributed to the changes in operating conditions.

Figure 4.3 is a visual description of the threshold resistance technique. The data provided were sampled at 50 kHz, and is plotted on a logarithmic resistance scale. The percent time the resistance was below each of the threshold resistance values was calculated for a full second of data and the results are displayed at the end of each arrow corresponding to the threshold resistance level. For example, the percent time the resistance was below the 10 Ω resistance level was 15.3 percent. Changes in the operating conditions that resulted in more interactions below this threshold resistance level would be indicated by a higher percentage than 15.3%. The threshold resistance levels chosen for this analysis were 1 Ω, 10 Ω, 50 Ω, 100 Ω, and 1000 Ω. The most useful information about surface interactions is described by the 1 Ω and 10 Ω levels. However, interesting data trends in the other levels give reason to include them as well.

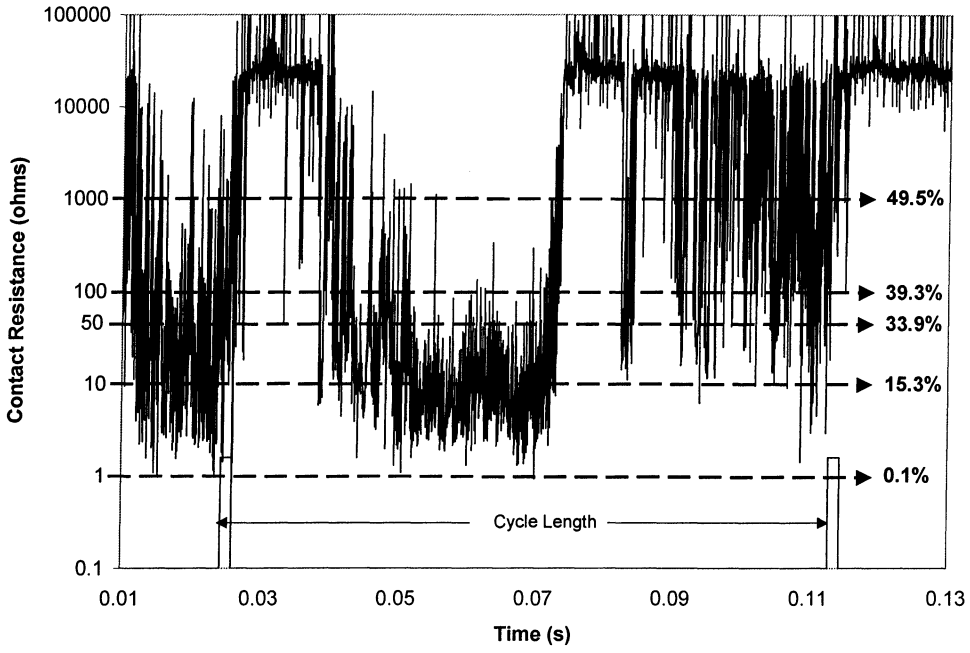

Figure 4.3 Threshold resistance applied to a contact resistance signal

4.2. Dynamic Pressure Data Reduction

The dynamic pressure microphone recorded the sound pressure dynamics within the cavity of the shoe/swashplate interface. The signal was visually inspected for changes during different conditions, and was also analyzed using other reduction techniques. It was anticipated

that changes in the signal would occur during scuffing interactions, however, conditions of low oil return to the compressor also brought out changes in the recorded signal.

The changes observed in the signal are described as events, since they have a large amplitude and short duration. Ten evenly spaced events were recorded each revolution, with varying magnitude. The source of these events is unknown, however, the five dual-headed piston compressor performed ten evenly space compression cycles per revolution.

To analyze the signal, initially an FFT of the signal was performed. Unfortunately, the signal is time varying, so the signal changes could not be detected by looking at the frequency content of the entire signal. This led to the use of wavelet analysis techniques. Wavelet decomposition investigates local frequency content as the signal progresses, and was an effective tool in detecting these changes in the dynamic pressure signal.

4.3. Acoustic Emission Data Reduction

The acoustic emission sensor was housed on the outside of the compressor casing to detect stress waves travelling on the surface as a result of scuffing at the shoe/swashplate interface. During steady oil return flow to the compressor, the acoustic emission sensor detected ten evenly spaced events. These events were recorded using the SoMat™ data acquisition system and therefore, the RMS signal was sampled. Each event corresponded to a discontinuity, or cusp, in the signal. The slope after each cusp relates to the intensity of the acoustic event, and these slopes varied between events.

The reliability of these events appearing under steady oil conditions was not high. Also, during failure of the compressor, no acoustic emission events were detected. Therefore, this technique was not pursued as an effective sensor in detecting oil film breakdown.

Chapter 5. Experimental Test Procedures

Many tests were performed on the compressor instrumentation described above. The results included here are meant to validate only the contact resistance measurement technique as a method to describe changes in the state of lubrication of the compressor during various steady lubrication regimes. The purpose of this chapter is to describe how steady lubrication conditions were established and maintained during these tests. The assembly techniques described here applied to all test cases.

5.1. Compressor Instrumentation

The assembly of a swashplate compressor uses several unique fixtures to ensure proper alignment and easier installation of the piston/shoe/swashplate components. Appendix D describes the instruction provided by Ford to properly assemble the compressor. This discussion will include the necessary modifications to their instructions to accommodate the instrumentation utilized in this study.

The dynamic pressure transducer was installed in the outer wall housing with the use of a mounting block, described in Appendix A. The transducer was mounted in the outer housing prior to any other assembly steps. The flush mounting to the inside surface of the outer housing prevented any interference with the inner housing during assembly. Instructions for mounting the dynamic pressure transducer can be found in Appendix A.

The acoustic emission sensor was a mounted on the compressor after all other assembly had been completed, and, therefore, did not interfere with compressor assembly instructions. The method for mounting the acoustic emission sensor is described in Appendix B.

The contact resistance instrumentation was the most involved assembly and required only minor adjustments to the assembly instructions of the compressor. Before a compressor can be assembled for a contact resistance measurement, the insulating Teflon™ pads previously described must be mounted to the piston bridges. This step requires machining the piston bridges and gluing the Teflon™ pads in place. Also, the instrumented piston, inner housing, and outer housing must be machined per the drawings included in Appendix C. Once the machining is complete, the nickel and gold plating were applied to the piston. Before plating the piston, it was necessary to remove the piston rings, and therefore, after the plating, new piston rings had to be installed. Once the pistons had been properly prepared and all necessary machining of the compressor was complete, assembly could begin.

Since the compressor was already assembled when purchased new, the sub-assembly instructions referred to in the Ford instructions of Appendix D did not apply. For example, the pins had already been installed in the valve plates. The compressor was shipped without oil, so oiling of the compressor components was necessary. The instructions to assemble the three-quarter pump, or inner housing, were followed. Next, this assembly was inserted into the outer housing.

At this time, the brush assembly was mounted to the inner housing through the outer housing. This required delicate placement of the brush into the grooves of the piston and fastening of three screws to attach the brush and brush block to the inner housing. Wires from the brush were attached to insulated pins through the outer brush cover. Insulated pins were necessary because this connection would short out the contact resistance circuit otherwise. This outer cover sealed the compressor and held the length of wires attaching the insulated pins. A small amount of Loctite™ sealant was used between the outer cover and the outside of the compressor housing to eliminate leakage. The four bolts that held the cover to the outside of the compressor provided sufficient force to seal the compressor.

Once the brush cover had been mounted, the compressor could be bolted together and the clutch assembly mounted as described by the Ford assembly instructions in Appendix D. Instead of using the bolt provided to hold the clutch on end of the compressor shaft, a longer bolt was fed through a machined mounting block and used to fasten the mounting block and clutch to the end of the compressor shaft. This mounting block was machined to the specifications of the slip ring. Two threaded holes provided mounting points for the slip ring and an additional threaded hole was used to connect the wiring to the end of the shaft. Once the necessary wiring was connected to the pins on the brush outer cover and to the slip ring, the compressor assembly was complete.

5.2. Loop Operation – Start Up Procedures

For all experiments using a compressor instrumented for contact resistance, the same start up procedures were followed to ensure unintentional damage to the swashplate did not occur. The loop was always operated in manual mode, which meant the Allen Bradley PLC controller described in Collins and Miller [1996] was not used. Instead, the control settings on the blowers, the compressor, and evaporator heater were set manually on the control units. All tests were done with similar operating conditions unless specific tests were being done. The following table describes the settings used:

Loop Component	Operating Set Point
Condenser Blower	45%, correlating to 1300 cfm
Condenser Re-circulation	0%, all condenser inlet air was room temperature
Evaporator Blower	55%, correlating to 290 cfm
Evaporator Heater	Sufficient to maintain 35 °C (95 °F)
Compressor Speed	13.3 Hz, or 800 rpm

Initially, there should be oil present throughout the loop, i.e. the shut down of the previous test was during steady oil circulation, especially in the suction line to the compressor. Although it was found that a lubricated compressor could run many hours without oil return the compressor, Chappell [2000], it was an unnecessary risk to damage an instrumented compressor, and was therefore avoided during startup.

When a previous test left the suction line to the compressor without oil, a compressor without instrumentation was run with steady oil circulation so that there would be sufficient oil in the suction line during the start up of the next test with the instrumented compressor. This was especially important after a compressor was disassembled, since it was unknown if the distribution of oil in the compressor was sufficient for operation without oil return until steady oil circulation was established.

It was also important to have oil in the suction line to the compressor, since the oil separator could not be started before steady operation had been established. This is a result of the physical limitations of the oil return loop. Since the separator was the helical type, any liquid from a two-phase evaporator exit condition would be collected in the separator. The result would be a low charge condition that would not damage the loop, but would cause problems during oil return. Therefore, during initial startup conditions, the bypass to the oil separator was used and the separator valves were closed to keep liquid refrigerant from collecting in the separator.

5.2.1. Charging the loop

Since the loop was often opened in between tests to exchange compressors, it was necessary to pull out the refrigerant after each test. This was done using a refrigerant recovery pump and a refillable refrigerant tank.

Charging the loop was done using the liquid line valve on a recovery tank connected to a refrigerant charging manifold. The high pressure gage line was connected to the liquid line of

the loop and the low pressure gage side was connected to suction line of the loop. Most of the charge entered the loop by opening the liquid line valve and heating the tank. The loop could be started once it contained at least 1.13 kg (2.5lbs.) of refrigerant.

The remaining charge was slowly pulled in using the suction line valve once the system was running. The typical charge level of the loop while running the oil separator was approximately 1.47 kg (3 lbs 4 oz.) The system was filled until the evaporator exit temperature was 16.7-22.2 °C (30-40 °F) above the evaporator inlet temperature. This would ensure that a two-phase condition would not occur at inlet to the separator.

5.2.2. Pre-heating the evaporator air loop

Preheating the evaporator air loop was necessary to avoid two phase conditions at the evaporator exit, and therefore the compressor suction line, during start up. This preheat was performed as the loop was charged.

As the refrigerant charge was added, the evaporator air loop was heated to 35 °C (95 °F). Once this was complete and the loop was charged, the loop was ready to be started. The heater has an automatic ramping feature to slowly bring the evaporator air temperature up. However, to save time, the manual setting on the heater was used. The evaporator blower must be on to operate the heater, recall the set point is 55%. Once it is started, the heater can be manually set to 20-25% to raise the temperature of the air loop. Care must be used during manual pre-heating, because the heating elements have a protection device that will shut off the heater if the device gets too hot. Therefore, the temperature of the air loop was monitored and the manual mode was turned off once the desired operating condition was met.

Once the heater obtained the desired 35 °C (95 °F) set point, the automatic control was used before the loop is started. Unfortunately, the response time of the heater control is not fast enough to keep up with the change in evaporator loading during startup of the loop. Therefore, immediately before startup, the heater should be manually set to 50%. Once the loop is started, the heater can be switched back to automatic mode. This is because without the loop running, the load on the heater to maintain the set point is low (~15%), but during loop operation the heater is much higher (~50%). Switching to manual mode to increase the output of the heater decreases the necessary response time of the automatic controller.

5.2.3. Separator operation

The loop was started using the bypass around the separator until stable operating conditions are reached. Next, the oil separator line was opened. Both separator ball valves were opened, and flow was permitted through both the separator and the bypass valve. Next, the bypass was closed. The increased loop volume may require more refrigerant to be added to maintain the desired evaporator exit conditions, but no more than 0.057 kg (2 oz) were typically necessary.

Once the separator was running, the oil return was started. To do this the ball valve between the separator and the oil return line was partially closed to induce the driving force for the oil. This valve was typically set at an angle of approximately 30 degrees from wide open. As a result, the pressure drop from the evaporator exit to the compressor inlet increased approximately 34.5 kPa (5 psi). The controlling needle valve was now slowly opened to control the amount of oil flow. Once operating, the flow of oil was slightly adjusted using either the pressure drop ball valve or the controlling needle valve. The mass flow meter in the oil return line measured the flow rate of the oil and was displayed on the PC with HP-VEE.

Before operating the oil return loop, there was no refrigerant in the oil return loop. However, as the concentration of refrigerant in this oil return loop increases, changes in the viscosity in the mixture in the oil return loop cause the mass flow rate returning to increase. Therefore the controlling needle valve must be occasionally closed to maintain the same amount of flow. A more detailed description of the oil return loop and the measurement of refrigerant in oil can be found in Chappell [2000]. The rate that oil absorbs refrigerant was slow, due to the low rate of oil exchange in the separator. It took several hours for a steady concentration of refrigerant in oil to occur in the separator return line.

5.3. Varying Steady Oil Return Tests

For steady oil return tests, first steady operating conditions were achieved using the techniques described above. The residual oil in the compressor did not get carried out quickly. Therefore, to detect changes in lubrication due to changes in oil return rate, it was important to start at the low oil circulation rate and increase to the maximum oil circulation rate.

5.4. Varying Compressor Speed During Steady Oil Return

Since automotive compressors are linked to engine speed, it was important to test various engine speeds to determine the effect on the state of compressor lubrication. For the three speeds tested, the oil return rate was held constant.

The tests were performed to determine the effect of increasing the loading on the shoe while maintaining a constant oil return rate. Unfortunately, the compressor speed affects more than the inertial loading of the shoe. By increasing the compressor speed, the increased refrigerant mass flow rate causes the condensing pressure to rise. Therefore, the shoe loading in the compressor increases through both inertial and pressure forces during this experiment.

To run this experiment, the system was brought to steady operating conditions as previously described. The compressor was initially run at 800 rpm. Compressor instrumentation data were taken until it appeared steady conditions had been reached. The compressor speed was then increased to 1600 rpm. As the system adjusted to this change, an increase in pressure in the suction line resulted in an increase in the oil return rate, so the controlling needle valve was adjusted to maintain the same oil return rate from the previous test. Again, instrumentation data were taken until it appeared steady conditions were present. Finally, the compressor was turned up to 2400 rpm. Again, as the system adjusted, the oil return rate was adjusted using the controlling needle valve to the same level as in the previous tests.

5.5. Varying Condenser Pressure During Steady Oil Return

To investigate another case of increased loading on the shoe, the condenser air inlet temperature was varied. The result was that the condensing temperature of the refrigerant increased, and therefore the condensing pressure increased. The resulting increase in the shoe loading was only a result of the increase in pressure difference across the compressor. The controlling needle valve was adjusted through the different conditions to maintain the same oil return rate.

The condenser air inlet temperature was controlled by the re-circulation baffle in the air loop duct. The baffle can be adjusted to bring in 100% room air to cool the condenser. After leaving the condenser, the air is forced out of the room through exhaust ducts. There exists a section of duct that connects the exit to the inlet. By adjusting the re-circulation baffle, the condenser inlet air can be a mixture of fresh room air and condenser discharge air. Therefore, the temperature can be controlled from room temperature and up. Three condenser air inlet temperatures were tested: 23.3, 28.3, and 35 °C (74, 83, and 95 °F). As a result of changing the

condenser air inlet temperature, the pressure rise across the compressor increased to corresponding levels of 668.8, 779.1, and 910.1 kPa (97, 113 and 132 psi).

Chapter 6. Instrumentation Verification Tests

To verify the correct operation of compressor instrumentation, several tests were performed. Verification of the contact resistance method is presented here. The dynamic pressure transducer and acoustic emission sensors were used to detect oil film breakdown during cases when low oil return was present and are discussed in more detail in Chappell [2000].

Since the measure of contact resistance between two sliding surfaces is an indirect measurement of the interactions between the surfaces, the surface roughness of the surfaces could change the level of contact resistance. As a result, surface profiles of the swashplate were taken to observe trends in the swashplate surfaces, as a new compressor was run-in. In addition, contact resistance data were taken during these tests to investigate measured trends during these profile changes.

Several other tests were performed to investigate changes in contact resistance during several steady operating conditions. The first was to investigate contact resistance trends with changes in steady oil return rate. The effects on contact resistance by varying the compressor loading by changing the compressor speed and changing the inlet air temperature to the condenser was also examined.

6.1. Compressor Run-In Tests

Measurements of surface profiles of the swashplate were taken to investigate run-in characteristics of the sliding surfaces. Three compressors were measured before they were used and after operating with a steady amount of oil return. During the run-in of these compressors, the steady oil return rate was held at 6.8-9.1 g/min (15-20 mlb/min) and the operating conditions were set for the idle compressor speed case (800 rpm). These compressors were labeled CR3, CR4 and CR5. The average roughness of the swashplate was measured several times to see how the run-in of the compressor swashplate occurred. Surface profiles were taken in the four locations described in Chapter 1 on all three new compressors before they had been run.

The compressor CR3 was run with steady oil return for 3.5 hours and a second set of surfaces profiles were taken. Again, the compressor was run with steady oil return and then a third set of surface profiles was taken. This test was repeated and another set of surface profiles was taken. The results of these surface roughness measurements are shown in Figure 6.1. The trend shows that before any wear of the compressor, the values of surface roughness are high and have a high amount of variability. The data taken after the compressor was run with steady oil

return show the values reaching a constant level and staying at that level. It is likely these data are the result of run-in of the compressor swashplate surface. Initially, the compressor was rough from the final finishing operations performed during manufacture. After some operating time, the swashplate surface was smoothed out by the shoes and reached a steady value.

The final set of data on shown in Figure 6.1 were taken after an oil shut off test. In this test, the compressor is run without oil return until failure occurs. A more detailed description of the oil shut off test can be found in Chappell [2000]. After failure, surface roughness was measure on the swashplate. One side of the compressor did not fail, and these are the final set of results included in Figure 6.1. The side that failed had surface roughness values near 1500 um, indicating significant surface interaction between the shoe and swashplate.

The summary of surface roughness provides good indication that the surface had reached a run-in condition after the first 3 ½ hour run in experiment. This is seen by the nearly steady level of surface roughness after the first 3 ½ hour experiment.

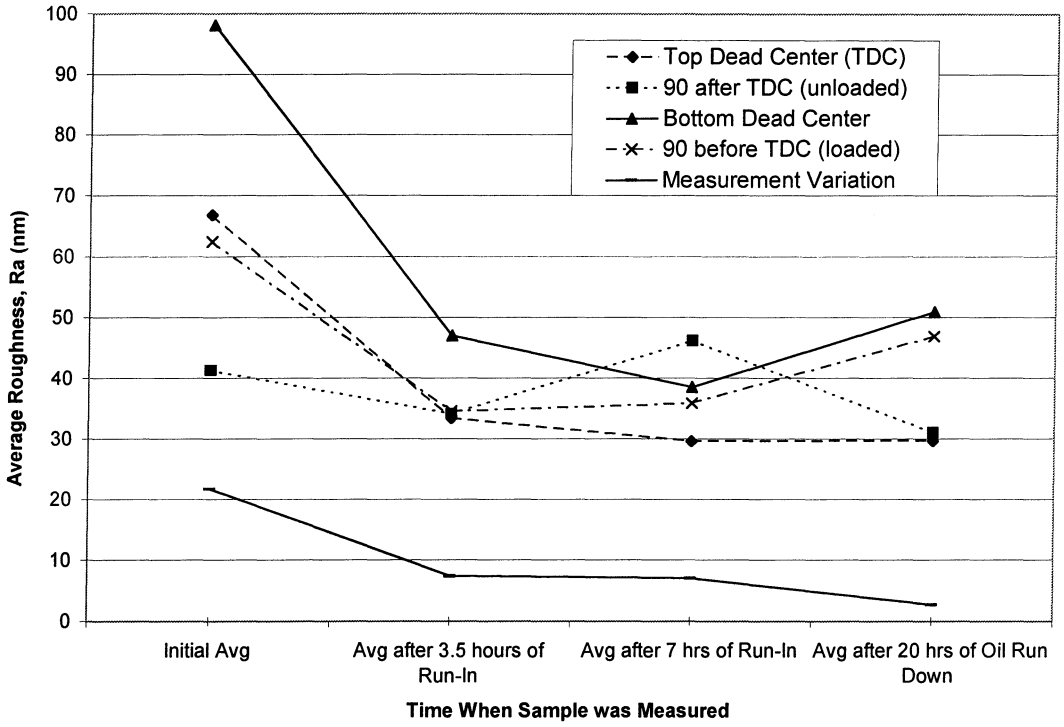

Figure 6.1 Surface profilometry results from run-in and oil shut off experiments of CR3

To provide further indication of this run-in time, surface profiles of two more compressors, CR4 and CR5, were performed. Initial profiles were taken, as well as profiles after 4 hours of operation with steady oil return. The results are summarized in Figure 6.2 (a-b). These results show the same trends as the first experiment.

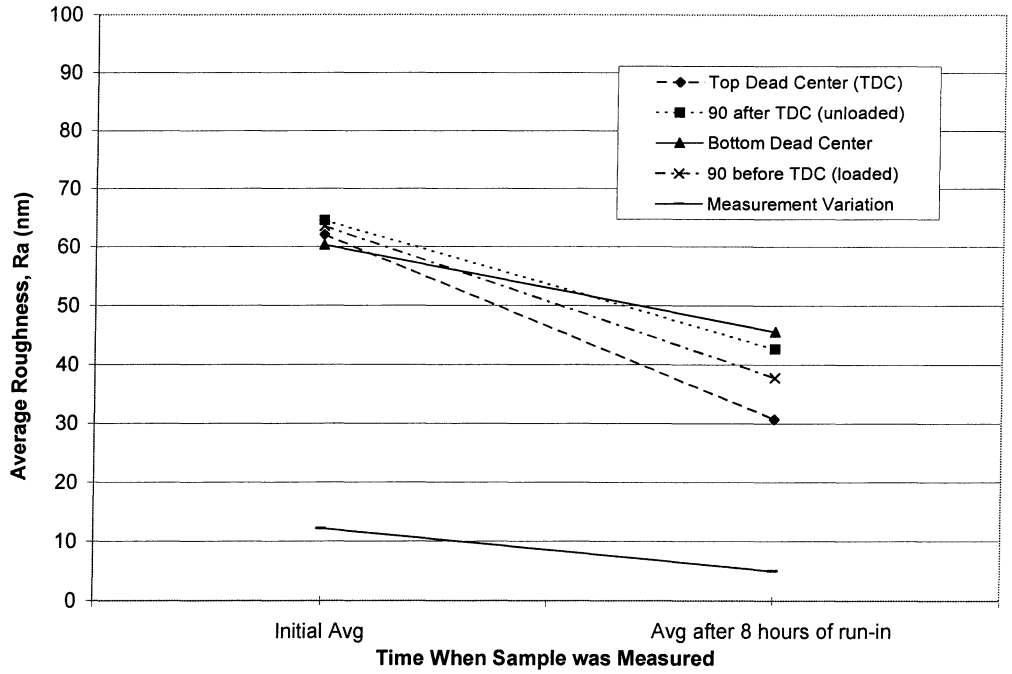

Figure 6.2 (a) Surface profilometry results of run-in experiments of CR4

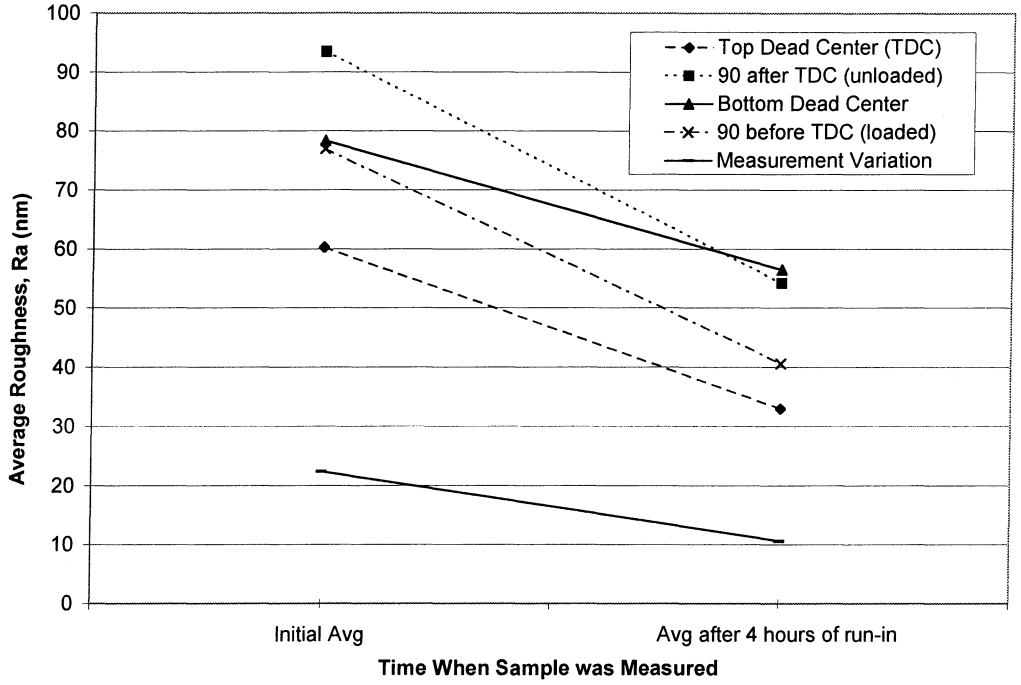

Figure 6.2 (b) Surface profilometry results of run-in experiments of CR5

Contact resistance results during the run in tests performed on CR4 and CR5 show trends indicating run-in, but could also be caused by system equilibrium processes. For example, the initial concentration of refrigerant in oil of the oil return line is near zero, and it approaches a steady system value after approximately one hour of operation time. Since the amount of

refrigerant in oil affects the viscosity of oil, this changing refrigerant in oil concentration could affect the values of contact resistance measured during this time. The threshold resistance data during each of these two run in experiments can be seen in Figures 6.3 (a-b).

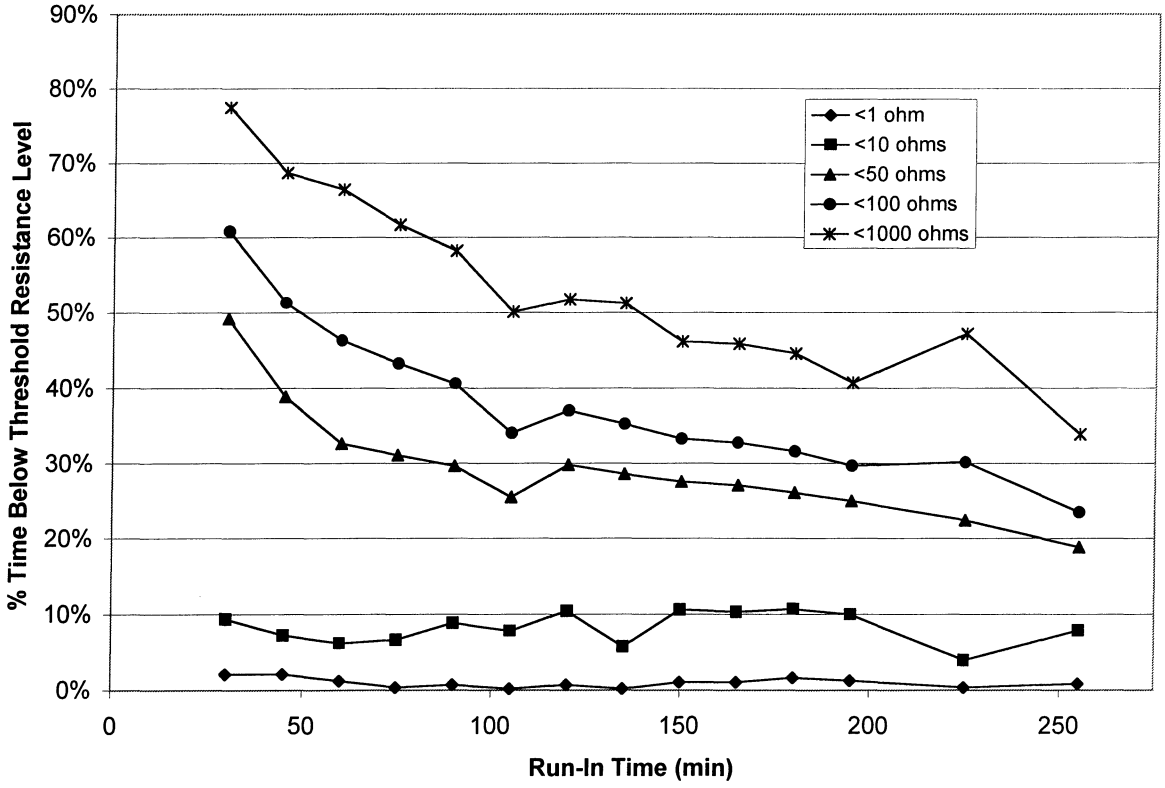

Figure 6.3 (a) Threshold resistance results from run-in experiments of CR4

In summary, the surface roughness values were measured on three new compressors and after some time run with steady oil return. Initially, the roughness values were high and spread out. After 3.5 - 4 hours of operation with steady oil return, the surface roughness dropped to a steady level until failure occurred.

6.2. Steady State Testing

Steady state oil circulation tests were performed to distinguish changes in the state of compressor lubrication as a result of changing the oil return rate to the compressor. The levels tested were chosen to determine the minimum threshold of steady oil circulation to the compressor. Unfortunately, the results show that for all levels of oil return tested, sufficient oil lubrication was present to prevent oil film breakdown from occurring.

There exists some ambiguity in determining the state of lubrication due to a certain oil return rate because of the capacity the compressor has to store oil. As a result, the minimum

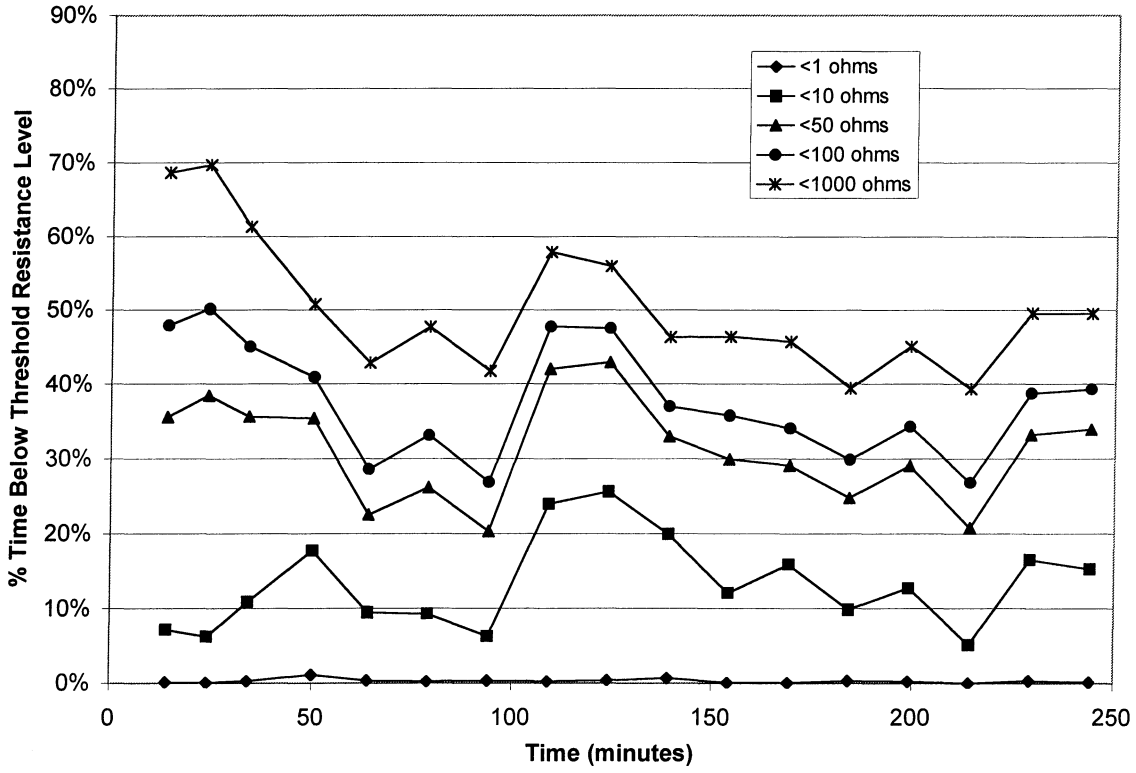

Figure 6.3 (b) Threshold resistance results from run-in experiments of CR5

level of oil circulation tested was 6.8 g/min (15 mlb/min). This level corresponded to a 0.5% circulation rate by mass. This was chosen as the minimum level to test because it was felt that below these levels the residual oil in the compressor became a dominant factor in determining the state of compressor lubrication. The effects of residual oil in the compressor were demonstrated during several tests performed where the oil return to the compressor had been shut off. These oil shut off tests are described in more detail in Chappell [2000].

The percent time resistance levels from the steady oil return rate tests from three instrumented compressors (CR0, CR4, CR5) are given in Figure 6.4. All three compressors were operated at the same idle speed of 800 rpm and similar operating conditions (evaporator exit superheat conditions, etc.). For most cases, the trend shows a decrease in the percent time resistance levels as the oil return rate increases. This can be explained by the decrease in surface interactions between the two sliding surfaces due to the increase in the amount of oil present that is a result of increased amount of oil returning to the compressor.

For one compressor, CR5, the percentage of time to resistance was below the threshold levels of 1 Ω and 10 Ω increased at higher oil circulation rates. Closer investigation of the data show one spot during the cycle where the resistance drops to values less than 1 Ω. The location

of the piston during the low values of resistance is at the top position of the compressor. As a result, it was suspected something was causing an unusually high load at this location. Investigation of the piston head after the test shows no visible signs of debris in the cylinder chamber. However, upon disassembly of the compressor, large amounts of residual oil were present in the cylinder (approximately 1-2 ml). An explanation is that the high rate of oil return left a large level of oil in the piston between compressions. The result of this excess oil in the piston caused a significant increase in the loading as it is forced through the small discharge valve opening. Further investigation is required to substantiate this hypothesis.

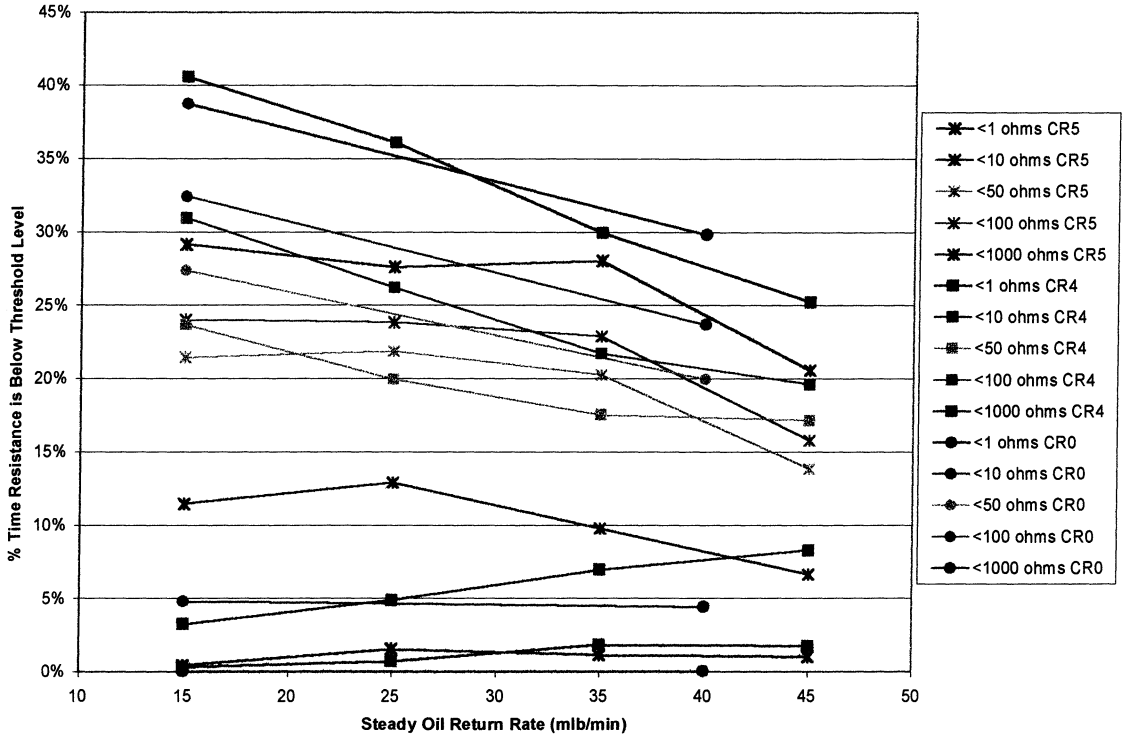

Figure 6.4 The effects of steady oil return rate on threshold resistance results

6.3. Compressor Speed Effects On Contact Resistance

For automotive air conditioning systems, compressor speed is a continuously varying parameter. As a result of increasing the speed of the compressor, the forces at the shoe swashplate interface increase. This is a result of both the inertial and pressure loads increasing.

Recall the equation from the simple model that described the piston loading effects on compressor speed:

$$F(t) = A\omega^2 \cos(\omega t)$$

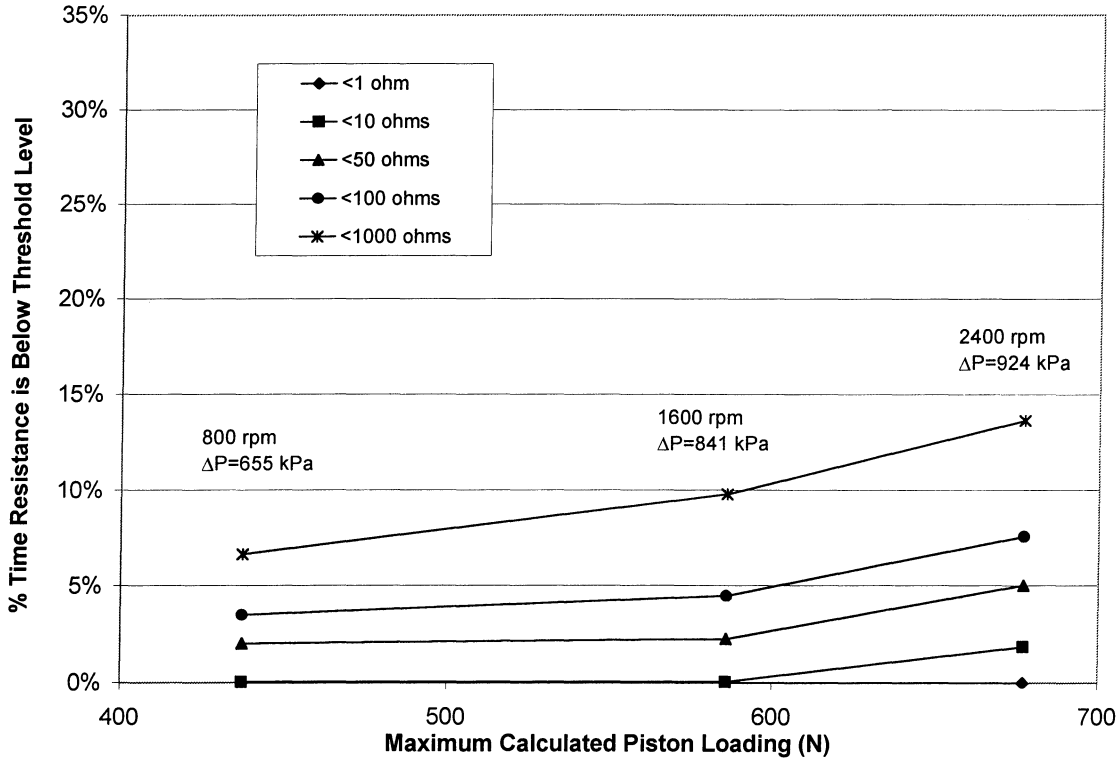

Figure 6.5 Compressor speed effects on threshold resistance values

This equation describes the strong effect increasing the speed of the compressor has on the force applied. However, at low speeds the pressure rise across the compressor is the dominating component of the shoe loading force.

The pressures in the system change due to the increase in mass flow rate of the system associated with increasing the compressor speed. Since the system has a fixed orifice expansion device, an increase in mass flow requires an increase in pressure drop across the orifice to increase the mass flow of the system. Therefore, as the speed of the compressor was changed, the resulting changes in the suction and discharge pressures were recorded to accurately produce new shoe loading curves for each condition.

To compare contact resistance data, the threshold resistance method for reducing the data was employed. The independent variable used in this plot was not compressor speed, instead it was the maximum shoe loading calculated using the shoe loading calculations. This is done to include the effects of changing the suction and discharge pressures with the compressor speed. Figure 6.5 plots the results of this test data performed on CR0. Steady operating conditions were achieved for each compressor speed without changing the oil return rate, which was held near 9.1 g/min (20 mlb/min). No changes were made from the set points described for steady operation in section 5.2 except for the compressor speed setting. The trend of the data show that

as the compressor speed increases, and therefore shoe loading increases, is the percentage of time the contact resistance is below each of the threshold resistance levels increases. In other words, as the loading increases at the shoe/swashplate interface, the contact resistance decreases.

6.4. Condenser Air Inlet Effects On Contact Resistance

During normal operation, the condenser air inlet temperature is an important operating condition. Since it can highly influence the condensing temperature, it determines the system operating pressure. As a result, the condenser air inlet temperature has a strong influence on the compressor shoe loading.

Three tests were performed continuously to determine the effect of changing the condenser air inlet temperature on the measured values of contact resistance during steady operating conditions. As previously described, the condenser air inlet temperature was controlled by adjusting the amount of air re-circulation in the condenser air loop. The minimum condenser air loop temperature is ambient air. Steady operating conditions were obtained with condenser air inlet temperatures of 23.3, 28.3, and 35 °C (74, 83, and 95 °F). For each steady case, operating conditions were recorded to calculate compressor shoe loading for each case.

The results were again plotted using the threshold resistance technique. The same maximum value of shoe loading is used as the independent variable (as was done for the variable compressor speed test results). These results are shown in Figure 6.6. Similar to the variable compressor speed tests, as the maximum shoe loading increases, the percent time contact resistance is below the threshold values also increases. Therefore, the increase in shoe loading results in lower values of contact resistance.

Notice that the initial condition between the two data sets were nearly identical, and the resulting threshold resistance levels were also quite similar. However, for the condenser air inlet test, there was a significant increase in the threshold resistance levels due to the increase in condenser air inlet temperature. There exists a large increase in threshold resistance levels from 23.3 to 28.3 °C (74 to 83 °F). The increase is less severe for the second increase in condenser air inlet temperature, but not as severe as in the first case. This may be a result of some other operating variables that were not monitored during this experiment. For example, the compressor may operate at a much higher temperature during conditions of high condenser air inlet temperature. A more detailed analysis of the compressor temperature distribution is necessary to consider this as a feasible explanation.

Observing the trends between increasing the condenser air inlet temperature and increasing the compressor speed, it appears the condenser air inlet temperature has much more severe effects on the measured levels of contact resistance. In fact, the change in compressor speed had very little effect compared with the condenser air inlet temperature trends. This trend describes the tolerance the swashplate compressor design has to the constantly varying speeds present in a mobile system. However, data were not taken at high condenser air inlet temperatures and varying compressor speeds, where it is like this trend will breakdown.

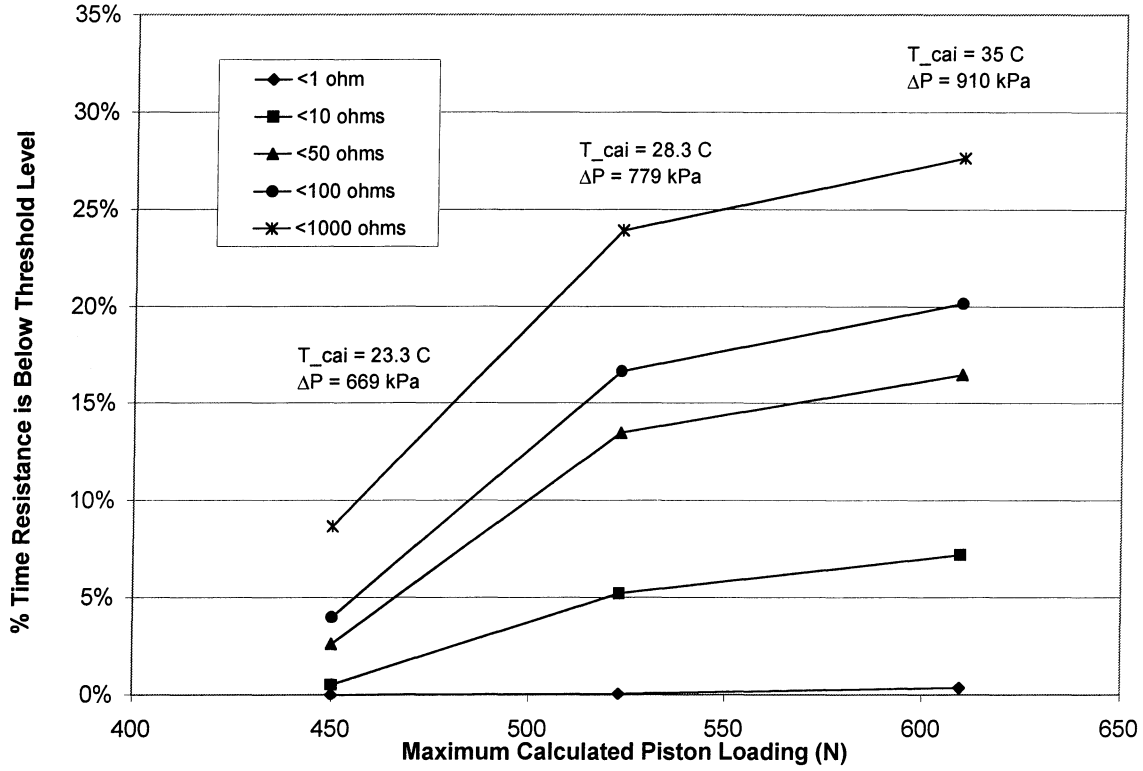

Figure 6.6 Condensor air inlet effects on contact resistance

Chapter 7. Conclusion and Additional Work

A real-time contact resistance sensor was used to measure contact resistance between the shoe and swashplate of an air conditioning compressor during steady oil return conditions.

The surface roughness measurements during run-in of the compressor showed that in less than 3 ½ hours of steady oil return, the surface had reached a steady surface roughness. This roughness was maintained until failure had occurred.

Results from steady oil return rates show that increasing the oil return rate increases the amount of time resistance is above 50 Ω, 100 Ω, and 1000 Ω, but that the time the resistance is below 1 Ω and 10 Ω remains fairly constant. Therefore, for the oil return rates tested, the amount of surface interactions did not change due to the change in oil return rate.

The effects of increasing the loading on the compressor were to increase the amount of time the compressor spent at lower values of contact resistance. The effects of varying the speed of the compressor on contact resistance levels appeared much less significant than the results of increasing the condenser air inlet temperature for the conditions tested.

Additional work with the contact resistance measurement was done during transient oil return conditions. Also included in those test data are the results of the dynamic pressure transducer and acoustic emission sensor. Two transient oil return conditions were tested that exist during startup. One was a result of refrigerant migration that has caused the oil in the compressor to be removed. The other is when liquid refrigerant in the suction line to the compressor results in slugging during startup conditions where the liquid refrigerant acts as a solvent and removes the oil from the swashplate surface. Both transient conditions exist briefly during start-up until oil return to the compressor is established, but the cumulative affects of these conditions can severely affect the life of a compressor.

Finally, a test was performed where the compressor was operated with steady oil return until steady state was reached, then the oil return was shut off. In this case, the oil in the compressor is slowly carried out by vapor refrigerant until insufficient oil is on the swashplate surface and failure occurs. The results of these transient tests as well as the methods used to control and measure oil circulation during these tests are discussed in detail in Chappell [2000].

Bibliography

Chappell, J, 2000: "Measurement of the Relationship Between Oil Circulation and Compressor Lubrication in a Mobile A/C System: Part Two." Department of Mechanical and Industrial Engineering University of Illinois at Urbana-Champaign, Master's Thesis.

Collins, C. D., N. R. Miller, 1996: "Experimental Study of Mobile Air Conditioning System Transient Behavior." Department of Mechanical and Industrial Engineering University of Illinois at Urbana-Champaign, ACRC TR-102.

Drozdek, J., J. Chappell, C. Cusano, P. Hrnjak, N. Miller, T. Newell, 2000:"Methods for Detection of Lubrication Failure Applied to a Swashplate Compressor." SAE Technical Paper 2000-01-0974.

Furey, M.J., 1961: "Metallic Contact and Friction between Sliding Surfaces." ASLE Transactions. Vol. 4, pp. 1-11.

Kioke, N., Y. Kumagai, K. Nakamura, 1998: "Development of Detection System for Abnormal Wear of Engine Bearings." JSAE Review. Vol. 19, pp. 27-32.

Meyer, J., J. Jabardo, 1994: "An Ultrasonic Device for Measuring the Oil Concentration in Flowing Liquid Refrigerant.: International Journal of Refrigeration. 17(7): 481-486.

Newell, T., 1996: "In Situ Refractometry for Concentration Measurements in Refrigeration Systems." HVAC&R Research. Vol. 2, No. 3, pp. 247-256.

Wandell, E., W. Dunn, N. Miller, and T. Newell, 1997: "Conditions That Limit Oil Circulation in a Mobile Air Conditioning System." SAE Technical Paper 98PC-21.

Weston, P., W. Dunn, and N. Miller, 1996: "Design and Construction of Mobile Air Conditioning Test Facility for Transient Studies." Department of Mechanical and Industrial Engineering University of Illinois at Urbana-Champaign, ACRC TR-128.

Yoon, H., and C. Cusano, 1999: "Scuffing Under Starved Lubrication Conditions." Department of Mechanical and Industrial Engineering University of Illinois at Urbana-Champaign, ACRC TR-147.

Appendix A: Dynamic Pressure Transducer Mounting Instructions and Mounting Block Drawing

The dynamic pressure transducer was used to detect sound pressure changes in the cavity of the compressor. To accomplish this, the transducer was mounted on the side of the compressor, in the top half of the outer housing. Figure A.1 describes the location of the pressure transducer. The pressure transducer was positioned opposite the contact resistance measurements due to space constraints on the outer housing. To mount the pressure transducer, it was necessary to machine a mounting block to hold the transducer in the desired location. This block was made to the necessary specifications of the pressure transducer, provided by the manufacturer.

The mounting block was held in place with two countersunk bolts that attached through the outer housing and into the mounting block. These two holes were sealed using Neoprene© o-rings. The microphone was sealed using a brass ring provided by the manufacturer. Brass rings of several sizes were provided to get the position of the sensor even with the inner wall of the outer housing.

When assembling the compressor, the pressure microphone must be mounted to the outer housing prior to assembly. This is caused by the limited access to the two countersunk bolts that hold the transducer mounting block in place. Once the pressure transducer is in place and the mounting bolts are tightened, assembly of the compressor can begin.

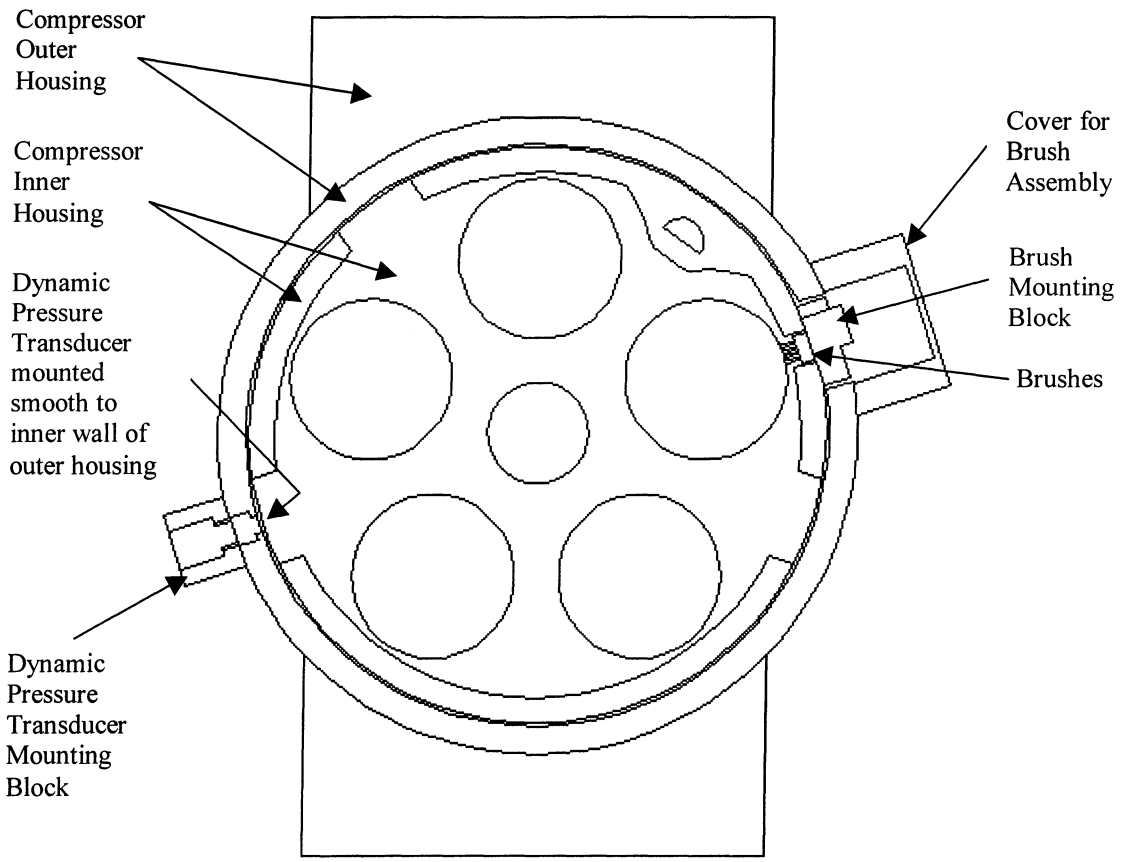

Figure A.1 Dynamic pressure transducer mounting block location on the compressor housing

Appendix B: Acoustic Emission Mounting Instructions

The acoustic emission sensor is designed to detect high frequency surface waves on a solid surface. To detect surface waves on the compressor housing, acoustic coupling was necessary. An area slightly larger than microphone (approximately 2 cm in diameter) was machined flat on the bottom side of the compressor housing (the bottom is the side opposite the clutch assembly). To provide the slight pressure necessary to hold the sensor to the surface of the compressor, several threaded bores on the compressor were used. These threaded bores were not used in the final assembly of the compressor, and were likely used during the fabrication and machining of the compressor. Using three bolts in these threaded bores, a small wooden block was held to the bottom of the compressor such that it could apply pressure on the acoustic emission sensor and hold the sensor in place.

The location of the sensor on the bottom of the compressor was not an optimized location. It was chosen based on its proximity to the bearing that would carry the signal from the swashplate to the outer housing.

Appendix C: Michigan Scientific Drawings for Contact Resistance Instrumentation

Michigan Scientific was contracted to design the electrical contact to the piston. Included are the drawings provided by them for the necessary machining of the compressor components. Figure A.1 describes the assembly of the brush assembly, brush block and cover for the brush assembly.

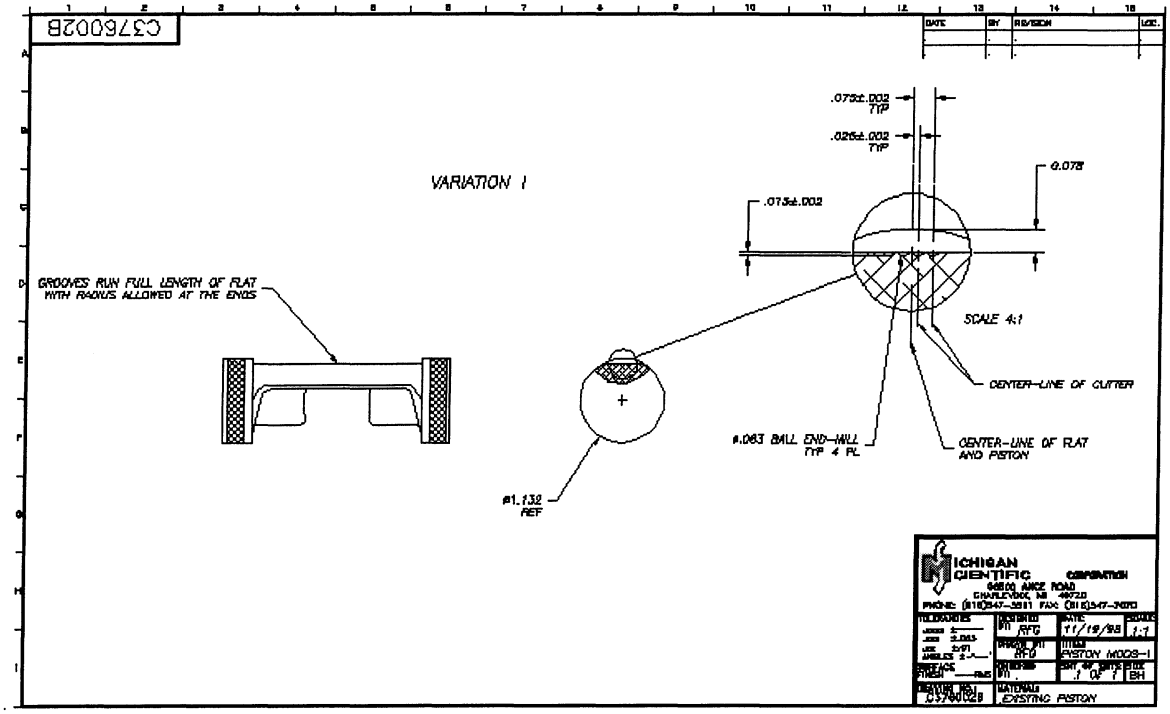

Figure C.1 Drawing of piston grooves

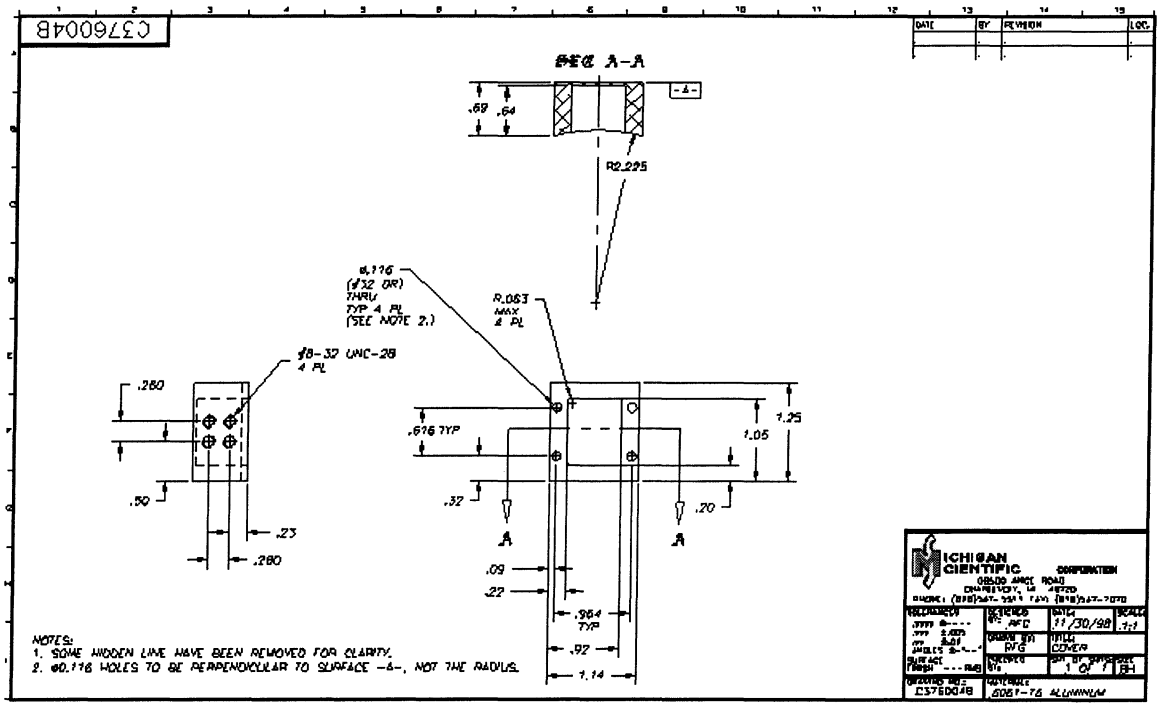

Figure C.2 Drawing of cover for brush assembly

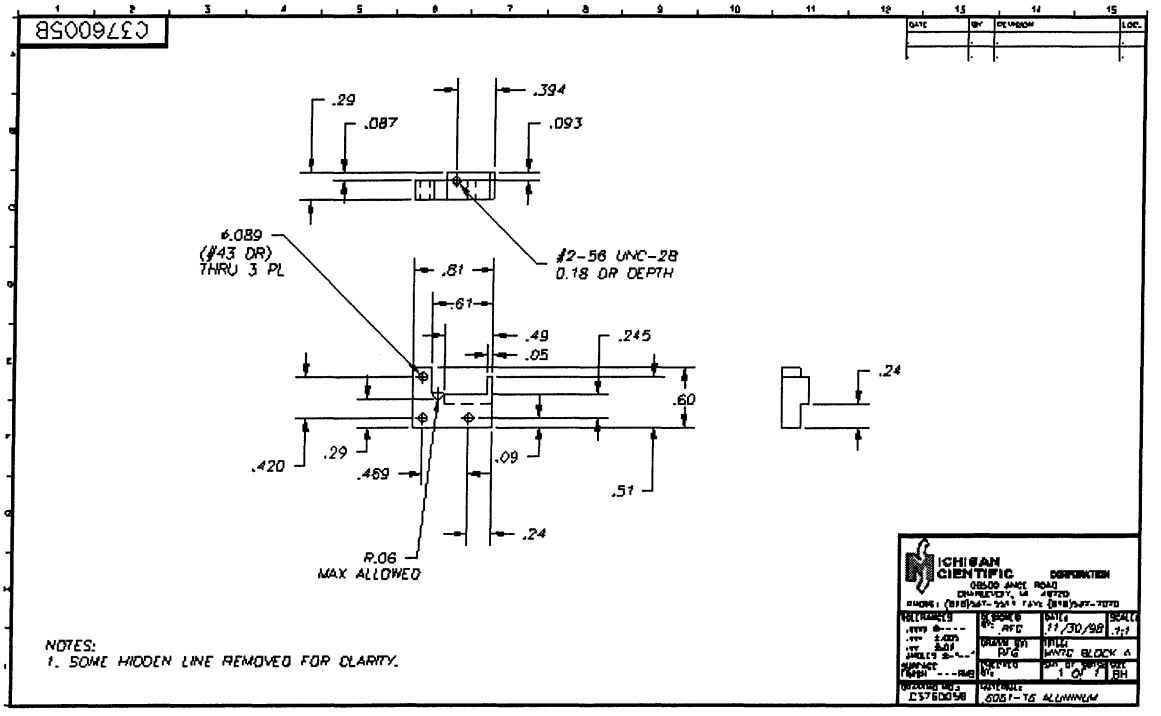

Figure C.3 Drawing of brush block

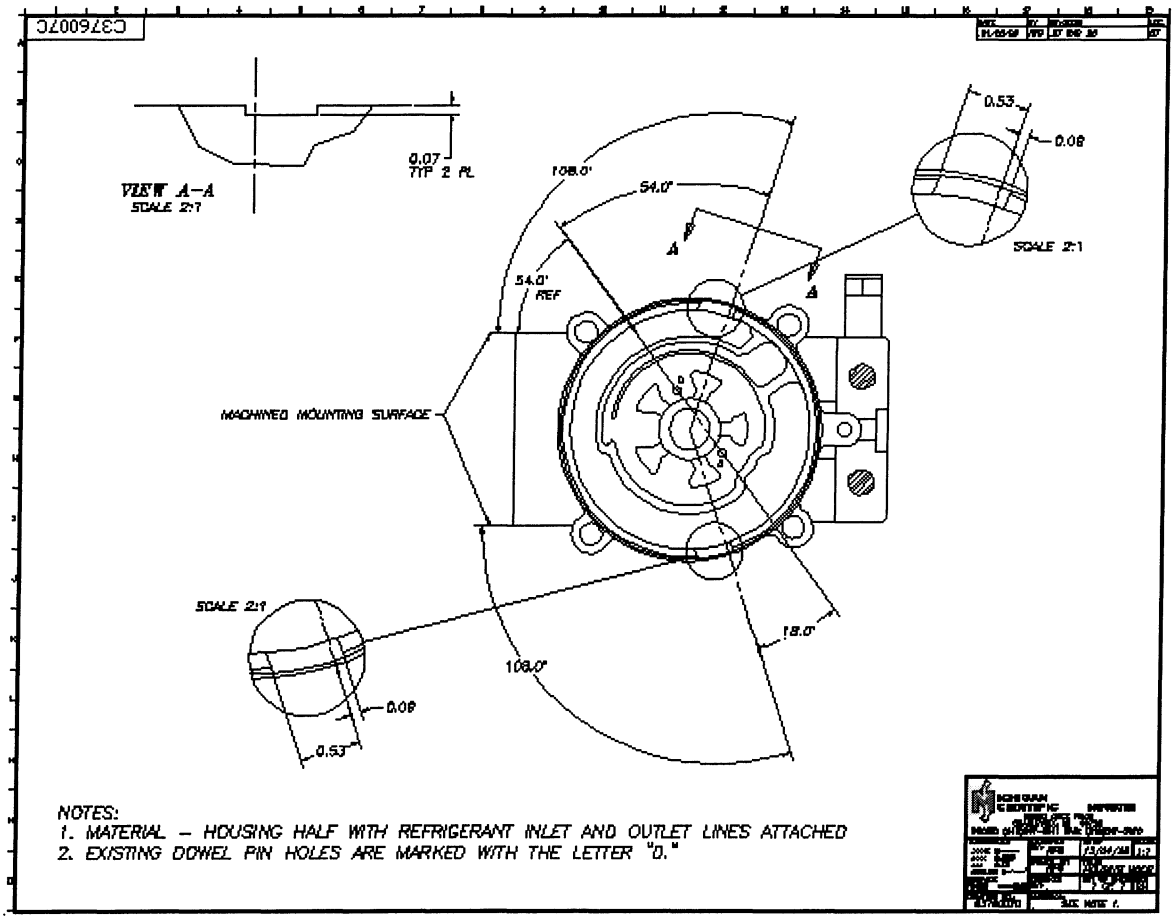

Figure C.4 Drawing of outer housing

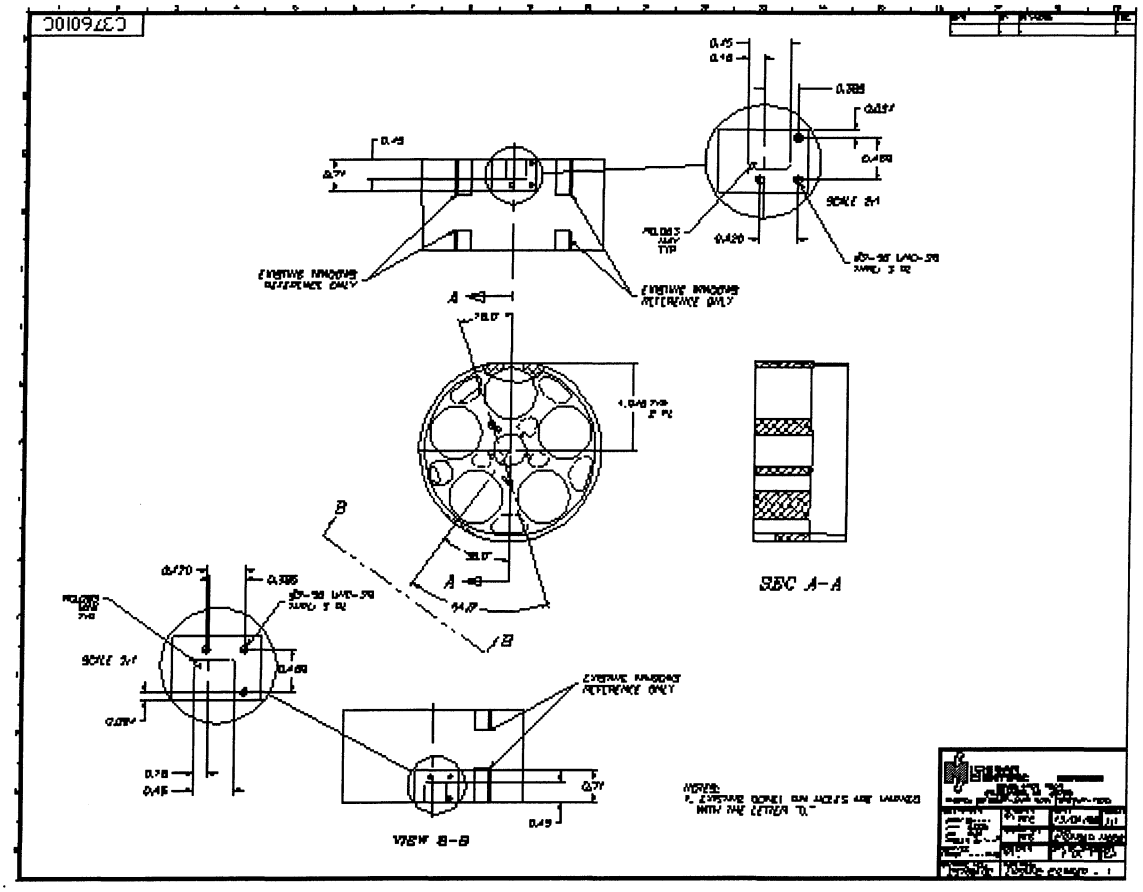

Figure C.5 Drawing of inner housing

Appendix D: Compressor Assembly Instructions (per Ford Motor Co.)

FS-10 Compressor Assembly Work Instructions

The following is a summary of the steps necessary to hand build the FS-10 compressor:

1. Subassembly & Measurements
2. Layout of Parts
3. Lubrication of Parts
4. Half Pump Assembly
5. Three Quarter Assembly
6. Head Bolt Torque
7. Initial Pump Up
8. Shaft Seal Insertion
9. Clutch Assembly
10. Preparation For Test

Note: Nitrile gloves should be worn when working with polyalkyleneglycol (PAG) oil. See Material Safety Data Sheet.

1. Subassembly & Measurements:
Perform the necessary subassemblies as documented in section three. After completion of subassembly, perform required measurements as documented in section four. With completion of both procedures, compressor parts are now ready for assembly.

2. Layout of Parts:
Layout necessary parts for assembly on bench. Parts that were measured previously, rack of pistons and shoes, swashplate assembly, front & rear thrust washers & bearings, front & rear cylinders and front & rear heads, are the main parts of assembly. The other components necessary are (2) valve plates, (4) pins (requires subassembly), (2) gaskets, (2) discharge reeds, (2) suction reeds, (1) head oring, (1) shaft seal, (1) felt, (2) manifold orings, (1) large & (1) small retainer ring, (4) head bolts, (1) clutch bolt, (1) manifold bolt, (1) manifold cover and clutch assembly.

3. Lubrication of Parts:
Place selected shoes into corresponding piston ball pockets. Using 16oz Nalgene container filled with Idemitsu FD46XG polyakyleneglycol (PAG) oil, squeeze approximately 5 drops onto shoes. Using same container squirt 3 to 4 drops into each piston bore & bushing of both cylinders. A Pyrex Peatree dish filled with the same oil is used for lubricating thrustwashers and front seal. Dip front washer set into dish and place on shaft, repeat with rear set. Lubricate front & rear of each valveplate with fingertips. Place discharge reeds onto chamfered discharge port sides only. Place suction reeds onto other sides of plates, then place gaskets over discharge reeds (with reed retainers facing up) and lubricate each side of both plates. Lubricate orings before setting into rear head, with fingertips also. When ready for shaft seal assembly, dip seal into peatree dish.

4. Half Pump Assembly:
To assembly half pump it is necessary to use piston/swashplate fixture. Fixture is numbered 1 through 5, front and rear. Swashplate is placed between shoes of each piston. Being careful not to drop shoes, assemble piston set number 1 first. Place forefinger between shoes then slip swashplate between them. Place the assembly into the fixture, with front of shaft facing the side of fixture marked front. Place pistons 2 & 3 onto swashplate, then place piston 5 finishing assembly with piston 4. Fold each side of fixture over. To complete half pump assembly front & rear cylinders are placed into piston/swashplate assembly. Place rear cylinder on first, with discharge half moon port opposite piston number 1 (on top of assembly). For ease of assembling rear cylinder, turn swashplate so pistons 1,2 & 5 are in front of 3 & 4. Place cylinder through shaft, into pistons, then remove assembly from fixture. Set assembly onto bench and place front cylinder through shaft into pistons, lining up both discharge ports.

5. Three Quarter Assembly:
Assembly three quarter pump with front & rear valveplate assembly, front & rear head and rear head oring. Place rear valveplate assembly into rear head, oring onto rear head, front plate assembly onto half pump and front head over rear head. For ease of placing rear plate assembly into rear head, place small finger through shaft and balance with thumb. Line up valveplate pins with opening of head and mate head and plate assembly. Place half pump into rear head, verifying alignment of dowel pins. Stretch lubricated oring onto rear head. Set front valveplate assembly through shaft, again lining up pins. Then place front head over assembly, lining up dowel pins, to complete the three quarter pump.

6. Head Bolt Torque:
Use compressor alignment fixture to align both heads of three quarter pump, (4) head bolts, shaft alignment tool and torquewrench (30 to 50 ft/lb). Place pump between four arms of fixture. Apply force to front head, making sure front head seats over oring. Place shaft alignment tool onto nose of pump, lining up both sets of splines. Conduct rotation check with tool. Place four bolts into heads, hand tighten. Torque bolts in four steps of 5 ft/lb increments, crossing over bolts diagonally, for a total of 18-20 ft/lbs. Rotate shaft tool between each step to properly seat pistons and maintain minimal run-out.

7. Initial Pump Up:
Place compressor into a vice to conduct initial pump up. Use ratchet and socket that fits onto shaft splines. Place finger over discharge port of rear head. Rotate ratchet and quickly turnover compressor to verify compressor builds up pressure.

8. Shaft Seal Insertion:
See shaft seal subassembly in Section 3. Use retainer ring pliers (Blue Point PR-12A) to place small retainer ring into nose of front head. Use lubricated front seal and felt for dust prevention.

9. Clutch Assembly:
Select required clutch assembly for testing. Use small green arbor and coil disc to press coil onto head. Use large retainer ring and external ring pliers (Blue-Point PR-38) to lock pulley in place. Also use clutch bolt, spacer for air gap, impact gun to tighten bolt, dial indicator to measure air gap, and 12V power supply to energize clutch. See clutch spacer measurement procedure in Section 4.
Decide which location coil connector should be pressed onto head. Place coil on front head, put coil disc on top and place into arbor. Press coil until seating completely on front head. Remove

to place pulley over coil. If pulley can not be placed on with palms of hands, slightly tap with soft mallet until going on completely. Lock pulley with retainer ring, select spacer and place on front of shaft. Put clutch plate over shaft, turn bolt into clutch and tighten with 8mm socket using impact gun. Specified torque for bolt is 8 to 10 ft/lbs. Check clutch air gap to verify .35 to .85mm. Usual air gap should be between .50 to .60mm.

10. Preparation for Test:
After proper air haps have been verified, place lubricated manifold orings into rear head and place manifold cover over them. Tighten with manifold bolt. Compressor is now ready.